Main Manuscript for

N6-Methyladenine DNA modification modulates pathogen virulence in nematodes

Authors: Dadong Dai[1,2]†, Shurong Zhang[1]†, Boyan Hu[1], Yayi Zhou[1], Simeng Cui[1], Jia Sun[1], Yali Zhang[1,2], Xueyu Wang[1], Shahid Siddique[2], Dexin Bo[1], Min Zhang[3], Valerie M Williamson[4], Haozhe Yao[1], Xinya Duan[1], Wentao Wu[5], Donghai Peng[1], Jinshui Zheng[1]*, and Ming Sun[1]*

Affiliations:
[1]National Key Laboratory of Agricultural Microbiology, Huazhong Agricultural University, Wuhan 430070, China; Hubei Hongshan Laboratory, Wuhan 430070, China.
[2]Department of Entomology and Nematology, University of California Davis, One Shields Avenue, Davis, CA 95616, USA.
[3]Wuhan Academy of Agricultural Sciences, Wuhan 430065, Hubei, China.
[4]Department of Plant Pathology and the Genome Center, University of California, Davis, CA 95616, USA.
[5]Key Laboratory of Agricultural Biodiversity and Pest Control, College of Plant Protection, Yunnan Agricultural University, Kunming, China.

*Ming Sun and Jinshui Zheng.

Email: m98sun@mail.hzau.edu.cn, jszheng@mail.hzau.edu.cn

Author Contributions: M.S., J. Z., and D. D. conceived the project. M. S., J. Z., D. D., and D. P. administration the project. M. S. acquisition the funding. D.D. designed the experiments. D. D., S. Z. performed the experiments. S. Z. purified the protein and performed the in vitro protein activity experiments. S. Z., J. L., and J. S. constructed the transgenic plants. D. D. collected the data and performed the data analysis. Y.Z. and B.H. performed the Dot blot experiments. D. D., S. Z., X. W., S. C., Y. Z., M. Z., B. H., G. W., W. W., and F. W. prepared the materials. D. D. wrote the manuscript, S. S., and V.M.W. revised the manuscript.

Competing Interest Statement: The authors declare that they have no competing interests.

Classification: Life Sciences/Molecular Biology/Epigenetics/DNA Methylation

Keywords: DNA 6mA, pathogen virulence, RKNs.

This PDF file includes:

Main Text
Figures 1 to 6

†These authors contributed equally to this work.

Abstract

Understanding the global regulatory mechanisms that control pathogen virulence gene expression is essential for elucidating the molecular basis of pathogenicity. N6-methyladenine (6mA) plays a crucial role in regulating gene expression in response to various environmental stresses; however, its role in pathogen virulence remains largely unexplored. Here, we report the widespread occurrence of 6mA across 17 nematode isolates and map its genomic landscape in six notorious agriculturally important pathogen root-knot nematodes (RKNs). We demonstrated that 6mA is characterized by a conserved GAG motif across nematodes, but exhibits species-specific distribution patterns and distinct effects on gene expression. In particular, its enrichment in transposable elements differs between polyploid and diploid nematodes, suggesting lineage-specific epigenetic regulation potentially associated with polyploidy. We further identified two functional 6mA demethylases, MiNMAD-1 and MiNMAD-2, and confirmed their catalytic activity and active sites. Host-induced gene silencing of minmad-1 significantly increased plant resistance to three polyploid RKN species. A detailed functional analysis revealed that minmad-1 knockdown disrupted virulence gene expression during the parasitic stage, thereby reducing nematode infectivity. Together, our findings suggest 6mA demethylase as a key epigenetic regulator of RKNs' virulence, providing new insights into nematode biology and offering promising targets for the development of sustainable control strategies.

Significance Statement

6mA methyltransferase regulates the expression of virulence genes in certain pathogenic bacteria and plays a critical role in their infectivity. However, the regulation of virulence gene expression in eukaryotic pathogens, particularly plant pathogens, remains poorly understood. Most studies on pathogen virulence have focused on individual effectors, with little insight into global regulatory mechanisms. Here, we demonstrate that 6mA broadly shapes virulence gene expression patterns in polyploid RKNs. Moreover, transgenic tobacco, tomato, and rice plants expressing dsRNA against nematode demethylases showed significantly enhanced resistance to RKNs. These findings establish 6mA demethylase as a promising epigenetic target for controlling plant-parasitic nematodes.

Main Text

Introduction

The regulation of pathogen virulence gene expression is crucial to understanding pathogenicity mechanisms. While current research has largely focuses on the functional analysis of individual virulence genes, little is known about the broader mechanisms underlying global virulence regulation in pathogens. DNA methylation, one of the earliest discovered DNA modifications, influences chromatin structure, DNA conformation, stability, and protein interactions, thereby modulating gene expression(1, 2). The role of 6mA in bacterial virulence is well established: DNA adenine methylase (Dam) is essential for *Salmonella* virulence(3), and Dam(-) mutants exhibit multiple virulence-related defects(4).

Dam also regulates effectors such as SpoA and SopB, the latter possessing phosphoinositide phosphatase activity(5, 6), and has also been reported to globally modulate the expression of cariogenicity-associated genes in *Streptococcus mutans*(7). Additionally, 6mA methyltransferase have been shown to regulate virulence gene expression in pathogenic bacteria that cause pediatric osteoarticular infections and enterocolitis(8, 9), as well as in the opportunistic pathogen *Pseudomonas aeruginosa*, which induces both acute and chronic infections(10). In *Streptococcus pyogenes*, 6mA also modulates the expression of Mga, a major transcriptional regulator of multiple virulence genes (11). In eukaryotes, evidence remains limited, with only a few studies reporting 6mA-regulated virulence in fungi. For example, 6mA methyltransferase is critical for the pathogenicity of the plant fungal pathogen *Cryphonectria parasitica*(12). However, most investigations linking 6mA to virulence have focused on animal pathogens, leaving its role in plant pathogens largely unexplored. Furthermore, while functional studies have predominantly examined 6mA methyltransferases, the roles of demethylases remain poorly understood.

Recently, DNA 6mA modification has been reported in an increasing number of eukaryotes, including *Caenorahabiditis elegans*(13), *Bursaphelenchus xylophilus*(14), *Drosophila*(15), *Chlamydomonas reinhardtii*(16), fungi(17, 18), plant(19-21), and mammal(22). In eukaryotes, 6mA methylation can occur in both symmetric and asymmetric contexts, while asymmetric 6mA methylation predominates in nematodes. Eukaryotic 6mA has been shown to be transmitted via a semiconservative mechanism(23) and incorporated into mammalian genomes by DNA polymerase(24, 25). Functionally, 6mA has been linked to disease onset(26-28), embryonic development(15), and environmental stress responses(20, 29). As a key epigenetic modulator, 6mA demethylases influences diverse biological processes, including eproduction(13), ovarian development(15), DNA replication and repair(30), vascular calcification(31), fatty acid metabolism in humans and mice(28), and neurodevelopment(32). The role of 6mA demethylase in pathogen infection has also been preliminary reported in *Mucor lusitanicus*(33). However, it is worth noting that several earlier studies reporting high 6mA levels in eukaryotes—especially mammals—were later shown to be confounded by bacterial DNA contamination(34). Thus, stringent control of bacterial contamination is critical for accurate detection of 6mA in eukaryotes.

Nevertheless, the mechanism by which 6mA regulates parasitism in eukaryotic pathogens—particularly the link between demethylases and virulence—remains unclear. Plant-parasitic nematodes (PPNs) cause devastating agricultural losses estimated to exceed $100 billion annually(35). Among them, root-knot nematodes (RKNs) are the most destructive(36), drawing increasing attention due to their broad host range and complex ploidy (37). Infective second-stage juveniles (J2s) penetrate host roots near the tip, migrate intercellularly, and establish giant cells within the vascular cylinder. These giant cells are extensively modified and serve as the sole nutrient source for nematodes throughout their lifecycle. A diverse suite of nematode effectors facilitate the formation and maintenance of giant cells(38). However, the epigenetic regulation of these effector genes remains largely unexplored. Previous studies of RKN epigenetics have mainly focused on histone modifications(39-41) and microRNA(42). Homology-based analysis of methyltransferases and

121 demethylases suggested that the *Meloidogyne incognita* (*M. incognita*, Mi) lacks DNA 6mA
122 modification machinery(43), raising doubts about the presence of 6mA in the RKN genomes.
123 Alternatively, these enzymes may have diverged substantially from known homologs,
124 warranting further investigation.
125
126 In this study, after rigorously eliminating bacterial DNA contamination, we investigated the
127 presence of 6mA in 17 nematode isolates using LC-MS/MS and confirmed DNA 6mA
128 modification in two diploids (*M. graminicola* and *M. hapla*), two allotriploids (*M. incognita* and *M.*
129 *arenaria* 3n), and two allotetraploids (*M. arenaria* 4n and *M. javanica*) through SMRT-seq,
130 N6-Methyladenine DNA immunoprecipitation sequencing (6mA-DIP-seq), and DNA Dot blot
131 assays. We found that 6mA is enriched in actively transcribed genes and exhibits distinct
132 distribution patterns across RKN species, particularly within transposable elements (TEs),
133 where striking differences were observed between diploid and allopolyploid RKNs. In M.
134 incognita, low-methylation-level sites were concentrated in the A2 subgenome and associated
135 with genes critical for cellular function, such as G protein-coupled receptors (GPCR).
136 Importantly, we identified two putative 6mA demethylases (MiNMAD-1 and MiNMAD-2) and
137 pinpointed their catalytic sites through structural prediction and biochemical validation.
138 Remarkably, host-induced gene silencing of *minmad-1* significantly enhanced resistance of
139 transgenic host plants to three polyploid RKN species. Further analyses revealed that
140 MiNMAD-1 globally regulates the expression pattern of numerous virulence genes. Collectively,
141 our findings establish a direct link between epigenetic regulation and virulence in a eukaryotic
142 pathogen.
143

144 **Results**

145 **6mA widespread in nematode genome**

146 To investigate the presence of DNA 6mA in nematodes, we analyzed 17 isolates, including
147 seven RKNs (*M. graminicola*, Mi, *M. arenaria* 3n, *M. arenaria* 4n, *M. javanica*, *M. enterolobii*,
148 and *M. hapla*), four isolates of *Heterodera glycines*, three migratory PPNs (*Aphelenchus*
149 *avenae*, *Ditylenchus destructor*, and *Bursaphelenchus xylophilus*), one animal-parasitic
150 nematodes (*Haemonchus contortus*), and two free-living nematodes (*Caenorhabditis elegans*
151 and *Caenorhabditis nigoni*). To minimize bacterial DNA contamination during liquid
152 chromatography coupled with tandem mass spectrometry (LC-MS/MS) detection, we
153 extracted DNA from sterilized eggs and verified the absence of bacterial contamination using
154 16S rRNA primers amplification(27F, 1492R) (see Method, *SI Appendix*, Fig. S1). Finally, a
155 clear 6mA signal was detected in all tested species (Fig. 1*A*).
156
157 To further understand the role of 6mA methylation in the life history of PPNs, we focused on
158 several species of RKNs (*SI Appendix*, Tables S1 and 2). PacBio sequencing is widely used to
159 detect 6mA modifications at single-base resolution; however, false positives caused by
160 bacterial contamination remain a major concern. To address this, we applied the 6mASCOPE
161 approach (34) to quantify potential contamination by aligning PacBio sequel I reads to the
162 NCBI nt database. The analysis showed that only 0.0004%-0.11% of reads were of bacterial
163 origin (*SI Appendix*, Tables S3). To further validate these estimates, we generated HiFi
164 sequencing data for Mi, Ma, and Mj and analyzed them with 6mASCOPE. The results revealed

that the proportions of fungal and bacterial reads were 0.018%, 0.011%, and 0.011%, respectively (*SI Appendix*, Tables S4-6). The 6mASCOPE evaluation confirmed that the contamination rate in our data was extremely low. We then analyzed the 6mA content in our previously assembled genomes of *M. graminicola* (Mg), Mi, *M. arenaria* 3n (Ma 3n), *M. arenaria* 4n (Ma 4n), and *M. javanica* (44) using PacBio sequel I data, and the results were consistent with the LC-MS/MS measurements. In addition, we generated a chromosome-level genome assembly for the diploid *M. hapla* (Mh, *SI Appendix*, Tables S7) using Pacbio, Illumina, and Hi-C data (*SI Appendix*, Tables S8). The genome size of this assembly is consistent with the previously reported version (45) (53.1 Mb vs. 53.6 Mb), but demonstrates markedly higher quality, as reflected by a substantially improved scaffold N50 (2.8 Mb vs. 0.08 Mb) and a BUSCO completeness of 66.8%. Furthermore, we identified 6mA modifications at single-base resolution in Mh using PacBio sequel I data. To minimize false positives, we excluded 6mA sites with low sequencing coverage, using different minimum coverage thresholds (ranging from 15× to 50×) depending on the sequencing depth of each sample, as previously described(13, 17). After this filtering step, numerous 6mA sites were identified across the six genomes (*SI Appendix*, Tables S9). Subsequently, to further minimize false positives in 6mA analysis, we performed whole-genome amplification (WGA) on the genomic DNA of Mi, Ma, Mj, Mg, and Mh. To evaluate the reliability of 6mA site detection, we used WGA samples sequenced by PacBio HiFi as negative controls. The number of 6mA sites identified in these WGA samples, which should not contain true methylation, reflects the false-positive rate (*SI Appendix*, Tables S9 and S10). We observed that samples with minimal bacterial contamination—such as Ma 4n—had very few false-positive 6mA sites. In contrast, WGA samples with higher contamination levels yielded substantially more false-positive sites (*SI Appendix*, Tables S10 and S11). These findings highlight the importance of controlling for contamination when interpreting 6mA methylation data.

To further validate the presence of 6mA in RKNs genome, we first excluded potential RNA m6A contamination (*SI Appendix*, Fig. S2, see Method). We then performed 6mA Dot blot assays on egg genomic DNA from Mi, Ma 3n, Ma 4n, Mj, Mg, and Mh, which all displayed clear 6mA signals (Fig. 1*B*, *SI Appendix*, Fig. S3). In contrast, no signal was detected in the negative control, in which nematode DNA was subjected to whole-genome amplification (WGA) using phi29 polymerase (Fig. 1*B*) or 18S amplification (*SI Appendix*, Fig. S3). We next applied LC-MS/MS to discriminate between 1mA from 6mA in these six genomic DNAs, and only 6mA signals were detected (Fig. 1*C*). Additionally, we performed 6mA-DIP-seq on Mi genomic DNA and Mi-WGA DNA (*SI Appendix*, Fig. S4*A*). Pearson correlation analysis confirmed high reproducibility between replicates (*SI Appendix*, Fig. S4*B*). The results verified the presence of 6mA in the Mi genome, with 53% of the peaks overlapping those identified by SMRT sequencing (*SI Appendix*, Fig. S4*C*, *D*). By contrast, only a few peaks were identified in the Mi-WGA 6mA-DIP-seq data (*SI Appendix*, Tables S12). Collectively, these results provide strong evidence for the presence of 6mA in RKN genomes.

6mA distribution landscape in nematodes genome

DNA methylation site distribution has been reported to be associated with gene expression regulation (46)**.** To comprehensively examine the regulatory effects of 6mA methylation on

gene expression in RKNs and the free-living nematode *C. elegans* (Ce, data download form GEO database, GSE66504), we categorized all 6mA-modified genes according to whether the sites were located in promoter, gene body, or distal intergenic regions. Most 6mA sites were found in gene bodies and promoters, with Ce showing the highest proportion of 6mA distribution in promoters (59.93%) (Fig. 2*A*; *SI Appendix*, Fig. S5). We then extracted 6mA sites from each of these regions and analyzed the 8-bp sequence flanking the modification sites for motif enrichment. Within a given species, the motifs of 6mA sites in promoters, gene bodies, and intergenic regions were largely similar (*SI Appendix*, Fig. S6). By contrast, cross-species comparisons revealed that motifs were highly conserved among RKNs but markedly different between RKNs and Ce (*SI Appendix*, Fig. S6). Specifically, the core motif in RKNs was GAG, whereas in Ce it was ApT, consistent with previous observations in fungi. This finding suggest that 6mA may regulate gene expression through distinct contexts in RKNs and Ce.

To investigate the functional implications of different 6mA methylation levels, we classified 6mA sites into three categories: low (at a specific locus, <30% of reads methylated across all sequencing data), moderate (30%-70%), and high (70%-100%). Moderate-methylation sites were the most abundant in Ce, Mi, Ma 3n, and Mj, accounting for ~76% of all 6mA sites. In Ma 4n, Mg, and Mh, approximately 50% of the sites showed moderate methylation, whereas only a small fraction exhibited high or low methylation (Fig. 2*B*). Motif analysis of the 8-bp flanking sequences revealed three distinct motifs corresponding to the methylation categories in each nematode (Fig. 2*C*). Among them, the GAG motif was most enriched at high-methylation sites in the four RKNs (Mi, Mj, Mg, and Mh), consistent with previous findings in *C. elegans*(13) and rice(19, 20). By contrast, motifs associated with moderate and low methylation levels varied considerably among species (Fig. 2*C*), suggesting that different levels of 6mA methylation may be regulated by distinct modifying enzymes and may serve diverse biological functions.

Subsequently, we analyzed the distribution density of 6mA sites in gene regions and transposable element (TE) regions across these nematode genomes. We found that the gene regions generally exhibited a low density of 6mA in all nematodes except Mh (Fig. 2*D*), a pattern reminiscent of the distribution characteristics of 5mC(19). By contrast, TE regions showed significant differences in the distribution density of 6mA sites between polyploidy and the diploid species (Ce, Mg, and Mh) (Fig. 2*E*). These observations suggest potential lineage-specific patterns of 6mA–TE distribution, which may warrant further investigation in the context of polyploidization.

To further investigate the distribution patterns of 6mA in TE regions of polyploid and diploid nematodes, we examined 6mA enrichment across different TE classes. In polyploid nematodes, 6mA was densely distributed in DNA transposons, MITEs, and LTRs, but showed a low density in low-complexity regions (*SI Appendix*, Fig. S7-10). We noticed that both the content and composition of TE differed significantly between polyploid and diploid RKNs (*SI Appendix*, Tables S13). In polyploid RKNs, TEs accounted for 28%-33% of the genome, with 8%-10% classified as Low-complexity elements (including simple repeat). While in diploid RKNs, only 8%-10% of the genome consisted of TEs, of which 41%-81% were low-complexity

elements. However, differences in TE composition alone cannot explain the pronounced discrepancy in 6mA abundance between polyploid and diploid nematodes. For instance, although diploid nematodes harbor a substantial proportion of DNA transposons, MITE-type Telements in these species still lacked the high-density 6mA modification observed in polyploids (*SI Appendix*, Fig. S11-13). For example, although *C. elegans* exhibits a TE composition similar to that of polyploid RKNs (*SI Appendix*, Tables S13), its 6mA distribution across TEs resembled that of diploid nematodes. To verify the authenticity of our observations, we repeated the analysis using false-positive 6mA sites predicted from WGA sequencing data. These false-positive sites showed neither increased density in the TE regions nor a decreased density in gene regions (*SI Appendix*, Fig. S14), but instead appeared randomly distributed across the genome. To further confirm the enrichment of 6mA in TE regions, we compared 6mA-DIP-seq peaks with the annotated TE regions in Mi. The results revealed that 74.8% of merged 6mA-DIP-seq peaks overlapped with the TE regions, whereas TEs comprise only 28.18% of the Mi genome. Together, these results indicate that the high-density 6mA feature of TEs in polyploid RKNs is not directly associated with TE type. Instead, it may reflect broader genomic processes, such as TE activity or mechanisms contributing to genome stability.

6mA regulates gene expression of RKNs

To assess the impact of 6mA methylation on gene expression, we examined the relationship between methylation status and gtranscrip levels from multiple perspectives. First, we compared the expression levels of 6mA-methylated and unmethylated genes in the egg stage (same stage as collecting SMRT sequencing data) across six RKN species. The results showed that in nearly all RKNs, 6mA-methylated genes exhibited significantly higher expression levels than unmethylated genes, whereas the opposite trend was observed in Mh (Fig. 3*A*). In polyploid RKNs, unmethylated genes were predominantly expressed at low levels (TPM<1), while a larger proportion of methylated genes displayed higher expression levels (TPM>5) (Fig. 3*B*). By contrast, in diploid RKNs, most genes—regardless of methylation status—showed expression levels exceeding TPM>5. In the free-living nematode Ce, however, the majority of genes exhibited low expression (TPM < 1) (Fig. 3*B*). Collectively, these findings suggest that 6mA methylation is associated with transcriptional activation in polyploid species, while no such trend is evident in diploid nematodes.

Subsequently, we performed motif enrichment analysis of 6mA sites in genes with TPM<1, 1<TPM<5, and TPM>5. The results showed that within the same species, genes across different expression levels exhibited similar motif enrichment patterns, and motifs among RKNs were relatively conserved, characterized by a core GAG motif (*SI Appendix*, Fig. S15). In contrast, a marked divergence was observed between Ce and RKNs, with the core motif in Ce being ApT (*SI Appendix*, Fig. S15). Notably, the motif patterns associated with genes of different expression levels are similar to those observed for 6mA sites located in different genomic regions, such as promoters, gene bodies, and distal intergenic regions (*SI Appendix*, Fig. S6).

Second, we examined genes modified by 6mA at only one of the three positions (promoter, gene body, or intergenic) as well as those simultaneously modified at all three positions (*SI*

297 *Appendix*, Fig. S16) to explore expression differences among these categories. The analysis
298 revealed that in polyploid RKNs (Mi, Ma 3n, Ma 4n, and Mj), genes methylated in the gene
299 body showed higher expression levels than the average of total genes (Fig. 3*C*). In contrast, in
300 diploid RKNs, promoter-methylated genes exhibited higher expression levels than the average
301 of total genes (Fig. 3*C*). Moreover, in Ce, both promoter- and gene body-methylated genes
302 were expressed at higher levels than the average of total genes (*SI Appendix*, Fig. S17), which
303 differs from the patterns in RKNs. These results suggest that 6mA exerts distinct regulatory
304 effects on gene expression in polyploid versus diploid RKNs, which may reflect differences in
305 ploidy level and reproductive strategy.
306
307 Third, we analyzed the expression levels of genes associated with different 6mA methylation
308 levels (low, moderate, and high). The results showed that in Mi, Ma 3n, and Mg, genes with
309 moderate methylation exhibited the highest expression levels, whereas in Ce and Mh, genes
310 with high methylation displayed the highest levels (Fig. 3*D*). These finding indicate that the
311 impact on gene expression differs among nematodes species.
312
313 Finally, we compared the expression levels of transposable element-related genes (TEGs) and
314 6mA-marked genes, as previously described(19). Genes unmodified by either 6mA or TE
315 shows the lowest expression levels in all six nematodes except Mh. The triploid RKNs (Mi and
316 Ma 3n) displayed similar patterns, whereas diploid and tetraploid RKNs did not (Fig. 3*E*). In Ma
317 3n, Ma 4n, Mj, Mg, and Ce, 6mA-modified genes with nearby TE showed higher expression
318 than those without, while the opposite trend was observed in Mi and Mh (*SI Appendix*, Fig.
319 S18). Moreover, 6mA-marked TEGs consistently exhibited significantly higher expression than
320 unmarked TEGs (*SI Appendix*, Fig. S18). These findings indicate that 6mA exerts
321 context-dependent effects on gene expression.
322
323 **Low-methylation-level 6mA sites play a crucial role in Mi**
324 We examined the genomic distribution of 6mA sites at different methylation levels in RKNs (*SI*
325 *Appendix*, Fig. S19*A*). Overall, sites of all three methylation levels were evenly distributed
326 across chromosome, except for low-methylation-level sites in Mi, which showed a distinct
327 enrichment (green circle in *SI Appendix*, Fig. S19*A*). Specifically, 72% of high-density-regions
328 (HDRs, >60 sites per 50 kb genome window) of low-methylation-level 6mA were located in the
329 A_2 subgenome. We then extracted genes from these HDRs in the A_2 subgenome, along with
330 orthologous regions in A_1, and B_1, to compare their expression level in egg stage. Notably,
331 the genes from A_2 consistently exhibited higher expression than those from A1 and B1 (*SI*
332 *Appendix*, Fig. S20). Moreover, these A_2 genes maintained higher expression not only in egg
333 stage (the stage used for 6mA profiling), but also across other developmental stages of Mi (*SI*
334 *Appendix*, Fig. S19*B*), suggesting a subgenome-specific regulatory role of 6mA.
335
336 To explore the functional differences of the genes associated with HDRs of
337 low-methylation-level 6mA sites between A_2 and the A_1/B_1 subgenome, we compared their
338 enriched Pfam domain. The results showed that the genes from A_2 subgenome were enriched
339 in GPCR (*SI Appendix*, Fig. S19*C*), consistent with previous GO enrichment results of the
340 genes with high methylation density in human(22). The GPCR superfamily represents one of

341 the largest chemoreceptor families; in nematodes, the absence of GPCR renders them “blind”
342 and “deaf” (47). GPCRs are also critical for fungal infection(48, 49) and may play essential
343 roles in host recognition and effector secretion in RKNs(50). Furthermore, GO analysis
344 revealed that A_2-associated genes were predominatly enriched in key molecule function, such
345 as pharyngeal gland morphogenesis in Mi (*SI Appendix*, Fig. S19*D*). These finding suggest
346 that low-methylation 6mA–modified genes in the A_2 subgenome participate in vital biological
347 processes and exert a stronger regulatory influence in A_2 than in A_1 or B_1 subgenome.
348
349 **MiNMAD-1/2 are involved in 6mA demethylation**
350 A previous study identified three 6mA methyltransferases from Mi, but the corresponding
351 demethylase remained unknown (43). To test whether Mi possesses 6mA demethylase activity,
352 we synthesized a biotin-labeled oligo DNA containing 6mA and measured its methylation level
353 after incubation with a suspension of disrupted Mi eggs. Compared with the heat-inactivated
354 egg suspension control and the BSA control, the 6mA content in the treatment group was
355 significantly reduced (*SI Appendix*, Fig. S21*A*), indicating the presence of one or more putative
356 6mA demethylases in Mi.
357
358 To identify putative demethylase genes in Mi, we collected six genes containing
359 2OG-FeII_Oxy_2 domain based on Pfam annotation, together with three genes showing the
360 highest sequence similarity to the *C. elegans* demethylase gene *nmad-1*. Phylogenetic
361 analysis revealed that these nine putative demethylase genes (including three alleles)
362 clustered into the *alkbh1*, *alkbh6,* and *alkbh7* families (Fig. 4*A*; *SI Appendix*, Fig. S22). To
363 assess whether these genes function as 6mA demethylases, we measured genomic DNA 6mA
364 levels after RNAi-mediated knockdown of each gene in Mi eggs using LC-MS/MS. The results
365 showed that knockdown of *Mi_14752.1* and *Mi_00010.1* significantly increased 6mA levels,
366 whereas knockdown of *Mi_23849.1* had no effect (Fig. 4*B*; SI Appendix, Fig. S21*B*).
367
368 We purified these three candidate proteins and tested their demethylation activity *in vitro.* Both
369 Mi_14752.1 and Mi_00010.1 were able to demethylate Mi genomic DNA (Fig. 4*C*, *D*; *SI*
370 *Appendix,* Fig. S23). To further validate their activity, we treated synthetic oligo DNA carrying
371 6mA modifications with the purified proteins, and again observed significant demethylation
372 activity for Mi_14752.1 and Mi_00010.1 (Fig. 4*E*). In addition, comparative sequence analysis
373 revealed that although demethylases from different species show substantial divergence at the
374 overall sequence level, their catalytic active sites are highly conserved (*SI Appendix*, Fig.
375 S24*A*). We predicted the 3D structure of Mi_14752.1, Mi_00010.1, Mi_23849.1, and
376 Ce_NMAD-1 using Alphafold2(51). Structural comparison revealed that Mi_14752.1 closely
377 resembles human ALKBH7, with a root-mean-square deviations (RMSD) of 0.067 Å (*SI*
378 *Appendix*, Fig. S24*B*). Moreover, the catalytic sites of Ce_NMAD-1 overlap with those of
379 Mi_14752.1 and Mi_00010.1 but not with Mi_23849.1 (*SI Appendix*, Fig. S24*C*-*E*). The RMSD
380 values between Ce_NMAD-1 and Mi_14752.1, Mi_00010.1, and Mi_23849.1 were 2.392,
381 1.066, and 12.625 Å, respectively (SI Appendix, Fig. S24*C*-*E*). To determine whether the
382 demethylase activity is intrinsic to Mi_14752.1 and Mi_00010.1, we introduced point mutations
383 (H153A and D155A in Mi_14752.1; H104A and D106A in Mi_00010.1). These mutations
384 completely abolition their demethylation activity (Fig. 4*F*). Accordingly, we designated

385 Mi_14752.1 as Mi N6-methyladenine demethylase 1 (MiNMAD-1) and Mi_00010.1 as
386 MiNMAD-2, reflecting their newly identified demethylation functions.
387
388 **Host-induced gene silencing (HIGS) of *minmad-1/2* reduces infectivity of MIG**
389 Considering that most stages of the RKN life cycle occur within plants, we generated
390 transgenic tobacco lines expressing dsRNA targeting *minmad-1/2, Mi_23849.1* (to verify its
391 demethylase activity during infection), and *gfp* as a control, to investigate the regulatory role of
392 6mA in parasitic stage of the *M. incognita* group (MIG, including Mi, Mj, and Ma). In three-week
393 pot experiments, *minmad-1/2*-HIGS tobacco plants exhibited significantly enhanced resistance
394 to Mi compared with *gfp*-HIGS and CK (wild-type) controls, whereas *Mi_23849.1*-HIGS plants
395 showed no significant difference (Fig. 5*A*). The eight-week pot experiment showed that the gall
396 number in the high-expression line of *minmad-1/2*-HIGS tobacco was reduced by
397 approximately tenfold compared with that in *gfp*-HIGS and CK plants (Fig. 5*B*; *SI Appendix*,
398 Fig. S25*A*, *B*). As anticipated, Mi genomic DNA exhibited a significant increase in 6mA levels
399 upon infestation of *minmad-1/2*-HIGS tobacco relative to the control (Fig. 5C), confirming the
400 demethylase activity of MiNMAD-1/2 in Mi. Subsequently, according to galls number, we
401 divided the nematode-infested *minmad-1/2*-, and *Mi_23849.1*-HIGS tobacco plants into three
402 groups including high-, medium-, low-galls groups (*SI Appendix*, Fig. S26*A*-*C*). After confirming
403 the absence of bacterial contamination (see Methods), DNA from females and eggs of the
404 three groups was extracted for 6mA quantification. The results showed a negative correlation
405 between 6mA content and gall number (Fig. 5*D*), indicating that demethylase silencing
406 reduces the virulence of Mi. Additionally, the 6mA level of females was much higher than that
407 of eggs (Fig. 5*D*), indicating a stage-specific difference in 6mA levels during development. To
408 further explore the resistance conferred by demethylase silencing in different hosts, we
409 generated *minmad-1*-HIGS tomato lines. Pot experiments demonstrated that RNAi targeting
410 the demethylase enhanced tomato resistance to Mi (*SI Appendix*, Fig. S27*A*-*C*), and the 6mA
411 level in Mi feeding on transgenic plants increased significantly (*SI Appendix*, Fig. S27*D*).
412 These results highlight the feasibility of using transgenic plants expressing Mi demethylase
413 dsRNA to confer resistance against Mi.
414
415 Additionally, *minmad-1* sequences are completely conserved among polyploid RKNs (*SI*
416 *Appendix*, Fig. S28), suggesting that the transgenic plants expressing Mi demethylase dsRNA
417 could potentially confer resistance to multiple polyploid RKNs. To test this hypothesis, we
418 evaluated the infection ability of other polyploid RKNs on transgenic tobacco. The results
419 showed that *minmad-1*-HIGS tobacco plants displayed significant resistance to the tetraploid
420 RKNs Mj and Ma 4n compared with CK and *gfp*-HIGS controls (Fig. 5*E*, *F*; *SI Appendix*, Fig.
421 S29*A*, *B*). Consistently, the 6mA levels of genomic DNA from Mj and Ma 4n were significantly
422 increased in *minmad-1*-HIGS group (Fig. 5*G*, *H*). Finally, to assess the role of demethylases in
423 diploid RKNs, we generated transgenic rice expressing Mg putative demethylase dsRNA.
424 However, these plants did not exhibit resistance to Mg, despite the significant elevation of 6mA
425 levels in nematodes feeding on them (*SI Appendix*, Fig. S29*C*-*F*). Together, these results
426 suggest that demethylases regulate the virulence of polyploid RKNs, whereas their functional
427 impact on diploid RKNs remains to be further explored.
428

429 **6mA regulates the expression pattern of the Mi virulence gene**
430 To further investigate the regulatory effect of the 6mA demethylase on Mi, we grew 80
431 *minmad-1*-HIGS tobacco plants inoculated with Mi. Based on gall formation, we divided the 80
432 tobacco plants into three categories: high-gall plants (groups 1–2, with numerous galls but
433 fewer than those in the control), medium-gall plants (groups 3–6), and low-gall plants (groups
434 7–8). Infective third/fourth-stage juveniles (J3/J4) were then collected from these three
435 categories for RNA-seq analysis (*SI Appendix*, Tables S14). We identified 7,198, 8,978, and
436 8,660 DEGs in high-, medium-, and low-gall plants, respectively (*SI Appendix*, Fig. S30).
437 Among them, 4,667 DEGs were shared across all three groups (*SI Appendix*, Fig. S31*A*) and
438 exhibited two distinct expression patterns (*SI Appendix*, Fig. S31*B*). The numbers of DEGs
439 unique to the high-, medium-, and low-gall plants were 832, 1685, and 1491, respectively (*SI*
440 *Appendix*, Fig. S31*A*). Functional enrichment analysis revealed that a large proportion of
441 downregulated DEGs unique to the medium-gall plants were ribosome genes (*SI Appendix*,
442 Fig. S31*C*), suggesting that demethylase activity may influence ribosomal function, thereby
443 modulating mRNA translation efficiency and ultimately reducing Mi infectivity.
444
445 To explore the primary cause of the reduced infectivity of Mi in *minmad-1*-HIGS tobacco plants,
446 we focused on the nematode's virulence gene (effectors), which constitute its key molecular
447 weapons for host parasitism. From the 4,667 DEGs shared by the three groups (high-,
448 medium-, and low-gall plants), we identified 520 putative effector genes (*SI Appendix*, Fig.
449 S31*A*). The putative effector genes exhibited consistently lower expression levels across all
450 three gall groups compared with the control (*SI Appendix*, Fig. S31*D*), with the low-gall group
451 showing the most pronounced downregulation (*SI Appendix*, Fig. S31*E*). These results
452 indicate a negative correlation between transgenic plant resistance and the expression levels
453 of Mi effectors.
454
455 Nematode invasion requires diverse effectors, and their proper expression is essential for host
456 infestation (52). Expression profiling revealed that all putative secreted protein genes clustered
457 into 11 groups, with RNAi plants displaying an expression pattern nearly opposite to the control
458 (Fig. 6*A*). These results indicate that demethylases globally alter effector expression, thereby
459 reducing Mi infectivity. To further examine the regulatory effect of demethylase on effectors, we
460 measured the expression of several reported nematode effectors in *minmad-1*-HIGS and
461 *gfp*-HIGS control tobacco plants by qRT-PCR. The results showed that, compared with the
462 *gfp*-HIGS control, the expression levels of Mi-XYl1, Mi-CRT, Mi8D05, MiPFN3, 16D10,
463 MiSGCR1, and MiIDL1 in female stage were markedly reduced, by approximately 22-fold
464 ($log_2FC = –4.46$), 126-fold ($log_2FC = –6.98$), 10-fold ($log_2FC = –3.32$), 28-fold ($log_2FC = –4.81$),
465 27-fold ($log_2FC = –4.75$), 5-fold ($log_2FC = –2.32$), and 13-fold ($log_2FC = –3.70$), respectively
466 (Fig. 6*B*; *SI Appendix*, Fig. S32; *SI Appendix*, Tables S15). To determine whether effector
467 reduction also occurred at the protein level, we generated a specific antibody against Mi-CRT.
468 Western blot analysis revealed that *minmad-1* RNAi significantly decreased Mi-CRT protein
469 accumulation compared with the gfp-HIGS and CK controls (Fig. 6*C*). Moreover, Mi-CRT
470 expression was down-regulated in both female and egg stages (Fig. 6*D*), suggesting that 6mA
471 DNA methylation may affect effector expression primarily at the transcriptional level, thereby
472 leading to reduced protein abundance.

We generated a specific antibody against the demethylase and performed ChIP-seq analysis on infective J2s to investigate whether the enzyme directly binds to and regulates effectors in polyploid RKNs (*SI Appendix*, Fig. S33*A*). The results revealed that 40.4%–51.7% of the candidate effector genes were bound by the demethylase (*SI Appendix*, Fig. S33*B-D*). We next performed 6mA-DIP-seq on Mi J2s to further assess whether 6mA directly marks the candidate effector genes. Approximately 40% of the candidate effector genes carried 6mA modifications, and notably, 47.4% of these overlapped with demethylase ChIP-seq targets (*SI Appendix*, Fig. S34). Together, these findings demonstrate that the enzyme directly acts on effector genes and may influence their transcriptional regulation.

Together, these results support a model in which 6mA methyltransferases and demethylases dynamically regulate effector methylation in a spatiotemporal manner, thereby shaping their expression across developmental stages (Fig. 6*E*). Such regulation likely represents a major epigenetic mechanism underlying the parasitic ability of RKNs. Importantly, whether 6mA also acts through transcription factors to exert broader control over effector networks remains to be determined, and will be an important direction for future research.

Discussion

In recent years, the existence of 6mA in eukaryotes has been debated, largely due to concerns about bacterial DNA contamination. To address this, we implemented multiple strategies to minimize false positives: (i) DNA was extracted from axenic eggs collected after nematode infection of axenic tobacco cultures; (ii) All tissues (egg, J3J4, female) were surface-sterilized with sodium hypochlorite and plated on LB and PDA media to confirm the absence of bacteria; (iii) 16S rRNA amplification showed no bacterial DNA bands; (iv) SMRT-seq reads were first aligned to nematode genomes and sites with ≥15× coverage were retained; (v) false positives were further excluded by sequencing WGA samples using PacBio and 6mA-DIP-seq; (vi) HiFi data analyzed by 6mASCOPE indicated bacterial/fungal contamination levels as low as ~0.01%; and (vii) LC-MS/MS distinguished DNA-derived 6mA from RNA-derived m6A. These results confirm that contamination in our datasets is negligible, strengthening the reliability of our findings. Nevertheless, when studying other nematodes—especially migratory parasites that feed on fungi or free-living species feeding on bacteria—greater caution is warranted. Our data further indicate that the egg stage, lacking intestinal tissues, is least prone to contamination. Importantly, WGA HiFi data also showed that samples with higher bacterial contamination yielded more false-positive 6mA calls, which may explain earlier misinterpretations of 6mA in eukaryotes. Our analyses verified that the contamination ratio was as low as 0.01%, supporting the high reliability of our results.

Methylation is an epigenetic modification that influences gene expression and genome stability. The enrichment of 6mA sites in transposable element (TE) regions may affect their stability, expression, and chromatin structure, thereby shaping the three-dimensional organization of the genome and modulating chromatin accessibility. Because TE regions contain highly repetitive sequences prone to recombination and insertion, they often contribute to genomic instability and mutation(53). However, 6mA methylation may enhance TE stability and reduce such structural changes, thereby preserving essential genetic information and supporting

517 species evolution and adaptability. Notably, while high-density TE methylation has been
518 associated with reduced expression of neighboring TE-related genes (TEGs)(54), our results
519 show that 6mA-marked TEGs exhibit significantly higher expression than unmarked ones.
520
521 Our results show that TE regions in polyploid nematodes harbor high-density 6mA methylation,
522 whereas diploid nematodes lack such enrichment. Given that TEs are often associated with
523 phenotypic diversity and stress responses (55), a comparative analysis of 6mA distribution
524 between polyploid and diploid RKNs may help uncover the mechanistic driving these
525 differences. Moreover, investigating the association between infection ability and 6mA across
526 RKNs of different ploidy could provide further biological insights. While we observed distinct
527 genomic and transcriptomic features between polyploid and diploid RKNs, these differences
528 may not be attributable to polyploidy alone. Polyploid RKNs included here are also more
529 closely related phylogenetically, raising the possibility that some features reflect shared
530 ancestry rather than polyploidy per se. Disentangling polyploidy effects from lineage-specific
531 adaptations will require broader taxon sampling, including both closely and distantly related
532 diploid and polyploid species. Future studies incorporating independent polyploidization
533 events and well-resolved phylogenies will be essential to clarify the respective roles of genome
534 duplication and evolutionary history.
535
536 The AlkB family of dealkylating enzymes is conserved from bacteria to humans(56, 57).
537 Humans encode nine AlkB proteins (AlkB1-8 and FTO), among which ALKBH1 and ALKBH4
538 are most strongly associated with demethylase activity. ALKBH1 has been confirmed as a
539 demethylase in human(22), mice(58), and rice(19), while NMAD-1 in *C. elegans,* a homolog of
540 ALKBH4, performs a similar role(13). In this study, we identified three proteins containing the
541 2OG-FeII_Oxy_2 domain from Mi. Our *in vivo* and *in vitro* assays demonstrated that two
542 proteins, homologous to ALKBH6 and ALKBH7, act as putative 6mA demethylases in triploid
543 Mi. Moreover, we found that genomic regions with different methylation levels corresponded to
544 distinct sequence motifs, suggesting that these motifs may be recognized by different
545 modifying enzyme systems.
546
547 Finally, our data suggest that 6mA can directly affect the expression of nematode virulence
548 genes, but it is also likely to influence virulence indirectly through modulating of key
549 transcription factors. Importantly, 6mA is a genome-wide epigenetic mark, and its role in
550 nematode biology extends beyond virulence regulation to broader essential processes such as
551 development, reproduction, and stress responses, consistent with its known effects on
552 shaping chromatin accessibility and transcriptional dynamics. Moreover, *minmad-1*-HIGS in
553 tomato and tobacco significantly enhanced the resistance to polyploid RKNs (Mi, Ma, and Mj),
554 whereas rice expressing Mg-demethylase dsRNA showed no resistance to Mg, and
555 demethylase knockout in *C. elegans* only modestly reduced egg-laying(13). These findings
556 suggest functional divergence of demethylase between polyploid and diploid nematodes,
557 potentially reflecting the greater importance of epigenetic regulation in parthenogenetic
558 compared to sexually reproducing organisms. Further studies of 6mA analysis in additional
559 parthenogenetic and sexual RKNs will be essential to further clarify its role across reproductive
560 modes and ploidy levels. In summary, this study establishes a link between epigenetic

561 regulation and pathogen virulence, and highlights 6mA as a promising target for nematode
562 control, with broader implications for the management of other agricultural pathogens.
563
564 **Materials and Methods**
565 **Nematode materials**
566 Our previously work has constructed the chromosome-level genome assemblies for *M.*
567 *incognita* WHF4-1, *M. arenria* SYMaF1-2, and *M. javanica* LongYF2-1., In addition, a
568 telomere-to-telomere assembly of *M. graminicola* (Mg) and a newly assembled genome of *M.*
569 *hapla* (Mh) were used in this study for subsequent 6mA DNA methylation analyses.
570 Nematodes were propagated on Rutgers tomato under greenhouse conditions at 25°C, and
571 eggs, J3J4 juveniles, and females were collected after six weeks for downstream experiments.
572 DNA used for SMRT-seq, LC-MS/MS and Dot blot assays was extracted from
573 surface-sterilized J2s inoculated into aseptically cultured tobacco grown in MS medium
574 solidified with plant gel instead of agar. After 35 days, sterile eggs were harvested for
575 subsequent analyses. Native DNA and WGA DNA used for HiFi sequencing and Mi-WGA
576 6mA-DIP-seq were obtained from eggs collected from nematodes infecting potted host plants.
577 Prior to DNA extraction, eggs were disinfected with 10% sodium hypochlorite to minimize
578 bacterial contamination. The protocol for stage-specific nematode collection is described in *SI*
579 *Appendix*, Materials and Methods.
580
581 **Nematode gDNA Extraction**
582 Genomic DNA was extracted from eggs of RKNs and cyst nematodes, as well as from
583 mixed-stage individuals of *D. destructor*, *A. avenae*, *B. xylophilus*, *H. contortus*, *C. elegans*,
584 and *C. nigoni* for subsequent experiments. Before DNA extraction, sodium hypochlorite was
585 used to sterilize the nematodes and pass through a 3 μm filter to remove contamination such
586 as bacteria. Genomic DNA isolation was performed as described in *SI Appendix*, Materials and
587 Methods.
588
589 **Eliminate bacterial DNA contamination and RNA m6A contamination**
590 To ensure the accuracy of 6mA detection in nematode DNA, multiple precautions were taken
591 to eliminate potential contamination from bacterial DNA and RNA-derived m6A. For all initial
592 tests, genomic DNA was extracted from nematode eggs. In root-knot nematodes, eggs were
593 collected from parasitized roots maintained under sterile tobacco culture conditions. To further
594 minimize bacterial contamination on the egg surface, eggs were disinfected with sodium
595 hypochlorite, then ground and plated on LB and PDA media to assess the presence of
596 cultivable endophytes. In addition, PCR amplification using universal 16S rRNA primers (27F
597 and 1492R) was performed on the extracted DNA to screen for bacterial DNA contamination.
598
599 To eliminate RNA contamination in downstream 6mA detection assays such as dot blot and
600 6mA-DIP-seq, genomic DNA was treated with RNase A following extraction. RNA fragment
601 sizes were monitored to confirm efficient digestion, with residual fragments reduced to less
602 than 100 bp. The DNA was then sonicated and size-selected with magnetic beads to retain
603 fragments larger than 200 bp. Finally, liquid chromatography–tandem mass spectrometry
604 (LC-MS/MS) was employed to distinguish DNA-derived 6mA (m/z 266.1 → 150.0) from

605 RNA-derived m6A (m/z 282.1 → 150.0), thereby confirming that the detected 6mA signals
606 originated exclusively from DNA.
607
608 **6mA-DIP-seq and analysis**
609 The 6mA-DIP-seq was performed following the published protocols. Briefly, we fragmented 7
610 ug WHF4-1 RNA removed gDNA to 200-400 bp. After end repaired and adapter ligation by
611 using Vazyme ND607 VAHTS Universal DNA Library Prep Kit for Illumina V3, DNA was
612 heat-denatured and immunoprecipitated overnight at 4 °C with anti-6mA antibodies purchased
613 from Abcam (ab151-230). Input and 6mA immunoprecipitated DNA was PCR amplified using
614 Vazyme ND607 to construction the next generation sequencing library. The raw data were
615 filtered by using Cutadapt (v3.3)(59) and aligned to WHF4-1 genome by using bowtie2
616 (v2.3.0)(60). The low quality and duplicate reads were removed by using SAMtools (v1.7)(61)
617 and Picard (https://broadinstitute.github.io/picard/). Then, macs2 (v2.1.1)(62) was introduced
618 to give the enriched regions to call 6mA peaks by comparing the reads between 6mA-IP and
619 Input sample, with the following options: -B -SPMR -nomodel. The post file was further
620 transformed into bigwig format for the profile visualization by using deeptools (v3.5.1)(63) and
621 IGV (v2.5.2)(64). The MEME-ChIP(65) (https://meme-suite.org/meme/tools/meme-chip) was
622 used to identify the conserved motifs enriched in 6mA peaks.
623
624 **DNA/RNA library construction and sequencing**
625 Approximately 100 μl eggs were purified and collected for DNA extraction, and the genomic
626 DNA was isolated using the CTAB method as described in previously. The DNA was sent to the
627 ANNOROAD Gene Technology Co., Ltd. (Beijing, China) for PacBio library construction
628 followed by sequel I platform sequencing. RNA extracting was using the TransZol Up Plus
629 RNA Kit (TransGen Biotech, Beijinng, China) and RNA Nano 6000 Assay Kit of the Bioanalyzer
630 2100 system (Agilent Technologies, CA, USA) was using to assess the RNA integrity and
631 concentration. The RNA library preparation was followed the protocol of VAHTS® Universal V8
632 RNA-seq Library Prep Kit for Illumina (Vazyme, Nanjing, China). Finally, the library was pooled
633 and sequenced on Illunima NovaSeq platform with 150 bp paired-end reads. Each treat of
634 RNA sequencing is performed by using three biological repetitions.
635
636 **Hi-C library construction and sequencing**
637 The eggs of Mh were used to construct the Hi-C library according to previously described
638 method with appropriate modifications(44). Briefly, approximately 50 thousand newly collected
639 eggs were pelleted and cross-linked in a 1.5% final concentration (v/v) formaldehyde (Sigma)
640 for 30 min, followed de-crosslinking, eggs were homogenized and digested by using MboI
641 (New England Biolabs). DNA was extracted after the addition of biotin, end-filling and ligation.
642 Subsequently, the DNA was sheared and removed from the unligated fragment ends biotin
643 mark by using T4 DNA polymerase. After biotinylated fragment pull-down, the target DNA was
644 used to construct the Hi-C library by using End Prep Mix 4 from VAHTSTM Universal DNA
645 Library Prep Kit for Illumina® ND607 (Vazyme, Nanjing, China), and then sequenced on
646 Illunima NovaSeq platform with 150 bp paired-end reads.
647
648 **Chromosome-level genome assembly**

649 To obtain a high quality Mh genome, through the Pacbio data, we performed de novo genome
650 assembly by using Canu (v1.9)(66) with default parameters. The initial assembled contigs
651 were polished with Illumina short reads for 5 rounds by using BWA (v0.7.17)(67), SAMtools,
652 sambamba (v0.7.1)(68), and pilon (v1.23)(69). Then, the Hi-C reads were aligned into the
653 corrected contigs by using Juicer (v1.5.7) pipeline(70). The 3D-DNA (v180419) pipeline(71)
654 was used to construct the chromosome-level scaffolds with parameter of -r 0, and we finally
655 obtained the MhF1-2 genome with 99.18% sequences clustered into 16 chromosomes.
656
657 **Genome annotation**
658 The egg, J2, J3J4, and female stages of Mh were collected to performed RNA-seq and
659 subsequently use to genome annotation. RepeatModeler(72) and RepeatMasker(73)
660 (http://www.repeatmasker.org) were used to soft-mask repetitive region of the assembled
661 genome. The RNA-seq data was aligned to the masked genome by using HISAT2 (v2.2.1)(74),
662 then, the BAM files were utilized to annotation based on ab initio prediction evidence by using
663 AUGUSTUS (v3.3.3)(75), GeneMark-ES (v4.64)(76), and BRAKER2 (v2.1.6)(77). On the
664 other hand, the RNA-seq data were de novo assembled using Trinity (v2.8.5)(78), and the
665 assembled transcripts were used to the following integrated by PASA (v2.4.1)(79). The file
666 augustus.hints.gff3 from Braker2 and the file pasa_assemblies.gff3 from PASA were used to
667 integrate all evidence to obtain a final gene structure information by using EVidenceModeler
668 (v1.1.1)(79). For the functional annotation, HMMER(80) was used to scan all the predicted
669 proteins conserve domains based on Pfam database, and eggNOG-mapper (v2.0.1)(81) was
670 used to perform the KEGG and GO annotation. For secreted protein prediction, we considered
671 the proteins with signal peptide but without transmembrane domain were secreted proteins.
672 The signal peptides were predicted by SignalP (v5.0)(82), and the transmembrane domains
673 were identified by using TMHMM (2.0c)(83). The transposable elements (TEs) were predicted
674 by using EDTA (v2.0.0) pipeline(84).
675
676 **6mA identification and analysis by SMRT sequencing**
677 We use SMRTLink-7.0.1 (http://www.pacb.com/support/software-downloads/) to identify the
678 6mA modification in WHF4-1, Mg, and Mh genome. The SMRT sequencing reads were aligned
679 to the genome by pbmm2, and the 6mA modification sites were identified by ipdSummary with
680 the following options: --methylFraction, --minCoverage 3, --identify m6A, --bigwig, --csv. The
681 6mA sites with less than 50 or 15 coverage were filtered according to the sequencing depth of
682 each RKNs as described before(13, 17). For motifs identification, the 6mA sites were
683 separated into three groups based on their methylation level (0-30%, 30%-70%, 70%-100%).
684 We extracted 4 bp from the upstream and downstream sequences of each 6mA site and used
685 BEDtools (v2.29.2)(85) to acquire the fasta file and followed by using MEME-ChIP to identify
686 motifs for each group. 6mA peaks were loading to R package ChIPseeker (v1.24.0)(86) for
687 associated genes annotation. The genome-wide distribution of 6mA sites with different
688 methylation levels was visualized using Circos (v0.69)(87). To calculate the reads
689 contamination rate of SMRT sequencing, we aligned the PacBio reads to bacteria, fungi, and
690 plant NCBI nt library, the aligned length more than 90% of the query reads were considered as
691 a valid alignment.
692

693 **6mA distribution density analysis**
694 The 6mA sites with different methylation levels were extracted into 6mAfilterHigh.bed,
695 6mAfilterMiddle.bed, and 6mAfilterLow.bed. We extended 4bp upstream and downstream of
696 the 6mA site to obtain the *_8bp.bed files for subsequent analysis. BEDtools bedtobam was
697 utilized to convert the *_8bp.bed files to *_8bp.bam files, and deeptools bamCoverage was
698 used to generate *_8bp.bw files from *_8bp.bam files. Finally, the BED files containing exon
699 and TE information, along with the *_8bp.bw files, were used to calculate the distribution
700 density of 6mA in the gene or TE region using computeMatrix, and plotProfile was employed to
701 visualize the results.
702
703 **DNA Dot blot**
704 The Hybond+ membranes were fully soaked in double distilled water, then soaked in 20 SSC
705 for 1h, sandwiched between two layers of filter paper and dried at 37 °C for 30 min. The
706 purified genomic DNA was heated at 95 °C for 5 min to denature DNA and immediately placed
707 on ice for 5 min and then 15 ng, 30 ng, and 50 ng DNA were loaded per dot on Hybond+
708 membranes. Membranes were air dry and placed them in the oven at 80 °C for 1 h, and
709 transferred into boxes with damp paper towels. DNA was then auto-crosslinked twice for 6 min
710 in an Ultraviolet crosslinker (CL-100). The membrane was blocked for 2 h in 5% skim milk
711 TTBS. Membranes were incubated overnight at 4 °C with 6mA primary antibody (ab151-230,
712 Abcam) in 5% skim milk TTBS. After three times wash for 5 min with TTBS, the blots were
713 probed with secondary antibody in 5% skim milk TTBS for 1 h at room temperature. Blots were
714 washed three times for 5 min with TTBS and then performed chemiluminescence detection.
715 After the chemiluminescence is over, the membrane is directly used for methylene blue
716 staining. (I) Immerse the membrane in 10mL of 1× methylene blue solution, stain for 3min on a
717 shaker at room temperature, and wash the membrane twice with double distilled water for 5
718 minutes each time; stain again with methylene blue solution for 3min and wash the membrane
719 twice with double distilled water for 5 minutes each time. Soak in TBST overnight at 4℃; (II)
720 Stain with methylene blue solution for 5min, wash three times with double distilled water for 5
721 minutes each time. Take photos in the gel imaging instrument/camera.
722
723 **LC–MS/MS analysis of 6mA**
724 The LC-MS/MS was performed as described before(13). Briefly, the nematodes genomic DNA
725 was denatured at 100 °C for 3 min, and chilled in ice for 2 min immediately. Aspirate 26 μl of
726 denatured DNA, add 1 μl of S1 nuclease, 3.2 μl of buffer, and treated at 37 °C overnight.
727 One-tenth volume of 1M NH_4HCO_3 and 1 μl venom phosphodiesterase I (Sigma) was added to
728 the solution and incubation at 37 °C for 2h. Finally, 1 U of alkaline phosphatase from *E. coli*
729 (Sigma) was added to the solution at 37 °C for 2h. The digested genomic DNA was diluted
730 two-fold with nuclease-free H_2O and filtered through 0.22 μm filter. To determine the peak
731 position of each nucleoside, the nucleoside standards including N6-methyldeoxyadenosine
732 and deoxyadenosine nucleoside were used to perform the reverse-phase ultra-performance
733 liquid chromatography on a C18 column (Agilent), with online mass spectrometry detection
734 using triple-quadrupole tandem mass spectrometer (Shimadzu, LC-MS 8050) set to multiple
735 reaction monitoring (MRM) in positive electrospray ionization mode. Simultaneous detection of
736 standards and samples using established methods base ion mass transitions of 266.1-150.0

737 for 6mA and 252.1-136.0 for A, and calculate the ratio of 6mA/A.
738
739 **RNA interference *in vitro***
740 We select about 300 bp conserved regions as RNAi target fragments. We synthesized dsRNA
741 using the T7 RNAi Transcription Kit-Box 1 (Vazyme, China, Cat. TR102-02). We followed the
742 protocol for dsRNA synthesis and diluted the concentration of dsRNA to 2 μg/μl. The potential
743 6mA demethylase in vitro interference experiment was performed using WHF4-1 eggs. About
744 10,000 WHF4-1 eggs were sterilized and suspended in 100 μl of nuclease-free water, and an
745 equal volume of dsRNA solution was added to make the final concentration of dsRNA to 1
746 μg/μl. After 60 hours of incubation at room temperature with 15 rpm rotation, the disturbed
747 eggs were divided into two parts, one was used for qRT-PCR to detect the interference
748 efficiency of the target gene, and the other was used to extract DNA to detect 6mA content by
749 mass spectrometry. Three biological replicates were performed for each experiment, dsGFP
750 was used as control.
751
752 **RNA-seq analysis**
753 The RNA-seq data of *C. elegans* were downloaded from SRA database (accession number
754 SRR6125151-SRR6125153). The raw reads of RNA-seq were cleaned by Cutadapt, the PCR
755 duplications were removed by using Picard. We use STAR [84] to align the reads to RKNs
756 genome and use RSEM(88) to calculate the TPM and FPKM value of each gene. For
757 differentially expressed genes (DEGs) analysis, HISAT2 was used to align the RNA-seq data
758 to the RKNs genome, then use SAMtools to convert the SAM files to BAM files and sort them,
759 and finally use HTSeq-count (v0.13.5)(89) to calculate the expression count number of each
760 gene. The count number was input into DESeq2 (v1.28.1)(90) to standardize and acquire the
761 DEGs. Differentially expressed genes (DEGs) were identified using DESeq2, applying an
762 adjusted p-value (FDR) < 0.05 and an absolute log2foldchange > 1 as thresholds.
763 Comparisons of gene expression (TPM) between groups were performed using the Wilcoxon
764 rank sum test, as TPM values showed non-normal distributions and unequal variances. Each
765 treatment was analyzed with three biological replicates. The expression module analysis of
766 secreted proteins was performed by using Mfuzz (v2.48.0)(91) and visualization by using R
767 package pheatmap (v1.0.12). The GO and Pfam enrichment analysis were performed by
768 python script and visualization by using R package ggplot2 (v3.3.3).
769
770 **Demethylase assays**
771 *In vitro* demethylase activity experiments were performed using purified potential demethylase
772 proteins of MiNMAD-1/2. The demethylase assays were performed as previously
773 described(13). In brief, a triplicate of a 50 μl volumes containing 1 μg WHF4-1 gDNA and 1 mg
774 recombinant protein in a reaction mixture (50 mM HEPES (pH 7.0), 50 mM KCl, 2 mM $MgCl_2$, 2
775 mM ascorbic acid, 1 mM α-KG, and 200 mM $(NH)_4Fe(SO)_4$) were used to perform the reaction.
776 After 1h hold at 37 °C, the reactions were stopped by adding 5mM EDTA and denatured at
777 100 °C for 3 min followed by chilling on ice for 2 min. The products of reactions were used to
778 Dot blot and LC-MS/MS to determine the 6mA contents after putative demethylase treated.
779
780 **Verification of endogenous nematode 6mA demethylase**

781 Verification of the nematode endogenous 6mA demethylase was carried out using protein
782 extracts from WHF4-1 eggs, followed by incubation with biotin-labeled oligo DNA and
783 pull-down with Dynabeads MyOne Streptavidin C1. The bound DNA was purified and analyzed
784 to assess demethylase activity. Detailed experimental procedures are provided in *SI Appendix*,
785 Materials and Methods.
786
787 **Polyclonal antibody preparation and western blot assays**
788 All the work of polyclonal antibody preparation was performed by Friendbio Science &
789 Technology (Wuhan, China). Briefly, the purified demathylase/Mi-CRT protein was used to
790 immunize rabbits intradermally for antiserum production, and gel specific purification was used
791 to purify the antibody. For western blot, the RKNs eggs, J2, and females were collected and
792 homogenate. The protein concentration of the suspended was determined by using the BCA
793 Kit (Beyotime, China). Proteins were separated on a 10% SDS-PAGE followed by blotting on
794 PVDF membranes (Biosharp, China). The membranes were blocked 2h in 5% skim milk TTBS
795 and probed with the demathylase/Mi-CRT antibody or β-actin (Proteintech, China, Cat No.:
796 66009-1-Ig) overnight. The secondary antibody and detection were performed as described in
797 Dot blot.
798
799 **Demethylase prediction**
800 We aligned the proteins sequence of WHF4-1 to the protein NMAD-1 of *C. elegans* by using a
801 loose e-values by using blastp (v2.10.1)(92). The first three proteins on the alignment were
802 selected as candidate demethylases. On the other hand, we performed Pfam domain
803 annotation on all the proteins of WHF4-1 and found that 6 of them have the 2OG-FeII_Oxy_2
804 domain with potential 6mA demethylase function. Every three of these 9 candidate genes are
805 alleles of each other, the coverage between alleles is 100%, and the minimum identity is 96%,
806 therefore, we selected one of the three alleles for further validation studies.
807
808 **Transgenic plant construct**
809 Nicotiana benthamiana was used to generate transgenic tobacco following the method of
810 Agrobacterium-mediated genetic transformation of leaf discs(93). We selected the same
811 segment as the above *in vitro* RNA interference as the segment for constructing transgenic
812 plants expressing dsRNA. The Agrobacterium EHA105 was inoculated into YEB medium and
813 cultured at 28 °C until OD600 up to 0.6-0.8. Put the tobacco leaf discs for about 6-7 weeks into
814 the Agrobacterium suspension and soak for 10min and culture in the dark at 28 °C for 2-4 days.
815 The explants were transferred to the Murashige and Skoog (MS) medium (with 1.0 mg/L
816 hormones Benzylaminopurine, 0.1 mg/L Indole acetic acid, 100 mg/L antibiotics kanamycin,
817 and 500 mg/L cefotaxime), and cultured under a light intensity of 25 μmol m^{-2} s^{-1} at 25 °C. After
818 4-5 weeks of selective culture, the explants will regenerate shoot buds and then transferred to
819 fresh selective medium. When the shoot buds grow to 3-4 cm, transfer to the rooting medium
820 (1/2 MS medium with the same concentration of antibiotics), and the roots will grow about 2-3
821 weeks. Using qRT-PCR to confirm putative T0 transgenic plants with specific primers
822 described in *SI Appendix*, Materials and Methods. Further, PCR-positive plant was cultured in
823 green house to obtain a homozygous T1 generation. Tomato transformation was performed
824 using the 'Moneymaker' cultivar, following the same method as used for tobacco

825 transformation. Cotyledons and hypocotyls from 5-day-old tomato seedlings were used for the
826 transformation. The rice transgenic was completed by Wuhan Towin Biotechnology Co., Ltd.
827
828 **Acknowledgements**
829 We thank Huazhong Agricultural University for technical support; Weiguo Lu of Henan
830 Academy of Agricultural Sciences for providing cyst nematode X12 material; Min Hu of
831 Huazhong Agricultural University for providing the *Haemonchus contortus* species; Xiaoli Guo
832 of Huazhong Agricultural University for providing the cyst nematodes Hg3 and Hg5 species;
833 Fengjuan Zhang of Hubei University for providing the *Aphelenchus avenae* and
834 *Bursaphelenchus xylophilus* species.
835
836 **References**
837 1. A. Zemach, I. E. McDaniel, P. Silva, D. Zilberman, Genome-wide evolutionary analysis
838 of eukaryotic DNA methylation. *Science* **328**, 916-919 (2010).
839 2. D. Wion, J. Casadesus, N6-methyl-adenine: an epigenetic signal for DNA-protein
840 interactions. *Nat Rev Microbiol* **4**, 183-192 (2006).
841 3. M. N. Giacomodonato, S. H. Sarnacki, M. N. Llana, M. C. Cerquetti, Dam and its role
842 in pathogenicity of *Salmonella enterica*. *The Journal of Infection in Developing*
843 *Countries* **3**, 484-490 (2009).
844 4. J. López-Garrido, J. Casadesús, Regulation of *Salmonella enterica* pathogenicity
845 island 1 by DNA adenine methylation. *Genetics* **184**, 637-649 (2010).
846 5. M. N. Giacomodonato *et al.*, Dam methylation regulates the expression of
847 SPI-5-encoded sopB gene in *Salmonella enterica* serovar Typhimurium. *Microbes and*
848 *Infection* **16**, 615-622 (2014).
849 6. M. N. Giacomodonato *et al.*, Impaired synthesis and secretion of SopA in *Salmonella*
850 Typhimurium dam mutants. *FEMS microbiology letters* **292**, 71-77 (2009).
851 7. J. A. Banas, S. Biswas, M. Zhu, Effects of DNA methylation on expression of virulence
852 genes in *Streptococcus mutans*. *Applied and environmental microbiology* **77**,
853 7236-7242 (2011).
854 8. Y. N. Srikhanta *et al.*, Phasevarion-regulated virulence in the emerging pediatric
855 pathogen *Kingella kingae*. *Infection and Immunity* **85**, 10.1128/iai. 00319-00317
856 (2017).
857 9. S. Falker, M. A. Schmidt, G. Heusipp, DNA methylation in *Yersinia enterocolitica*: role
858 of the DNA adenine methyltransferase in mismatch repair and regulation of virulence
859 factors. *Microbiology* **151**, 2291-2299 (2005).
860 10. S. Han *et al.*, DNA Methyltransferase regulates nitric oxide homeostasis and virulence
861 in a chronically adapted *Pseudomonas aeruginosa* strain. *MSystems* **7**,
862 e00434-00422 (2022).
863 11. T. M. Nye *et al.*, DNA methylation from a Type I restriction modification system
864 influences gene expression and virulence in *Streptococcus pyogenes*. *PLoS*
865 *pathogens* **15**, e1007841 (2019).
866 12. Z. Miao *et al.*, BcMettl4-mediated DNA adenine N 6-methylation (6mA) is critical for
867 virulence of *Botrytis cinerea*. *Frontiers in Microbiology*, 2155 (2022).
868 13. E. L. Greer *et al.*, DNA Methylation on N6-Adenine in *C. elegans*. *Cell* **161**, 868-878

869 (2015).
870 14. Z. Liu, Y. Li, X. Zhang, DNA methylation on C5-Cytosine and N6-Adenine in the
871 *Bursaphelenchus xylophilus* genome. *BMC genomics* **24**, 671 (2023).
872 15. G. Zhang *et al.*, N6-methyladenine DNA modification in *Drosophila*. *Cell* **161**, 893-906
873 (2015).
874 16. Y. Fu *et al.*, N6-methyldeoxyadenosine marks active transcription start sites in
875 *Chlamydomonas*. *Cell* **161**, 879-892 (2015).
876 17. S. J. Mondo *et al.*, Widespread adenine N6-methylation of active genes in fungi. *Nat*
877 *Genet* **49**, 964-968 (2017).
878 18. C. Lax *et al.*, Symmetric and asymmetric DNA N6-adenine methylation regulates
879 different biological responses in *Mucorales*. *Nature Communications* **15**, 6066 (2024).
880 19. C. Zhou *et al.*, Identification and analysis of adenine N(6)-methylation sites in the rice
881 genome. *Nat Plants* **4**, 554-563 (2018).
882 20. Q. Zhang *et al.*, N(6)-Methyladenine DNA Methylation in Japonica and Indica Rice
883 Genomes and Its Association with Gene Expression, Plant Development, and Stress
884 Responses. *Mol Plant* **11**, 1492-1508 (2018).
885 21. Z. Liang *et al.*, DNA N(6)-Adenine Methylation in *Arabidopsis thaliana*. *Dev Cell* **45**,
886 406-416 e403 (2018).
887 22. C. L. Xiao *et al.*, N(6)-Methyladenine DNA Modification in the Human Genome. *Mol*
888 *Cell* **71**, 306-318 e307 (2018).
889 23. Y. Sheng *et al.*, Semiconservative transmission of DNA N6-adenine methylation in a
890 unicellular eukaryote. *Genome Research* (2024).
891 24. X. Liu *et al.*, N6-methyladenine is incorporated into mammalian genome by DNA
892 polymerase. *Cell research* **31**, 94-97 (2021).
893 25. C. Lyu *et al.*, Rare and misincorporated DNA N6-methyladenine is a hallmark of
894 cytotoxic stresses for selectively stimulating the stemness and proliferation of
895 glioblastoma cells. *Cell Discovery* **8**, 39 (2022).
896 26. Q. Xie *et al.*, N(6)-methyladenine DNA Modification in Glioblastoma. *Cell* **175**,
897 1228-1243 e1220 (2018).
898 27. C. Shen, K. Wang, X. Deng, J. Chen, DNA N(6)-methyldeoxyadenosine in mammals
899 and human disease. *Trends Genet* **38**, 454-467 (2022).
900 28. L. Luo *et al.*, DNA 6mA Demethylase ALKBH1 Orchestrates Fatty Acid Metabolism
901 and Suppresses Diet-Induced Hepatic Steatosis. *Cell Mol Gastroenterol Hepatol* **14**,
902 1213-1233 (2022).
903 29. C. Ma *et al.*, N6-methyldeoxyadenine is a transgenerational epigenetic signal for
904 mitochondrial stress adaptation. *Nature Cell Biology* **21**, 319-327 (2019).
905 30. S. Y. Wang *et al.*, The demethylase NMAD-1 regulates DNA replication and repair in
906 the *Caenorhabditis elegans* germline. *PLoS Genet* **15**, e1008252 (2019).
907 31. K. Zhu, J. Reiser, ALKBH1 reduces DNA N6-methyladenine to allow for vascular
908 calcification in chronic kidney disease. *J Clin Invest* **131** (2021).
909 32. B. Yao *et al.*, Active N(6)-Methyladenine Demethylation by DMAD Regulates Gene
910 Expression by Coordinating with Polycomb Protein in Neurons. *Mol Cell* **71**, 848-857
911 e846 (2018).
912 33. M. Osorio-Concepcion, C. Lax, E. Navarro, F. E. Nicolas, V. Garre, DNA Methylation

913 on N6-Adenine Regulates the Hyphal Development during Dimorphism in the
914 Early-Diverging Fungus *Mucor lusitanicus*. *J Fungi (Basel)* **7** (2021).
915 34. Y. Kong *et al.*, Critical assessment of DNA adenine methylation in eukaryotes using
916 quantitative deconvolution. *Science* **375**, 515-522 (2022).
917 35. P. Abad *et al.*, Genome sequence of the metazoan plant-parasitic nematode
918 *Meloidogyne incognita*. *Nat Biotechnol* **26**, 909-915 (2008).
919 36. J. T. Jones *et al.*, Top 10 plant-parasitic nematodes in molecular plant pathology. *Mol*
920 *Plant Pathol* **14**, 946-961 (2013).
921 37. P. Castagnone-Sereno, E. G. Danchin, L. Perfus-Barbeoch, P. Abad, Diversity and
922 evolution of root-knot nematodes, genus *Meloidogyne*: new insights from the genomic
923 era. *Annu Rev Phytopathol* **51**, 203-220 (2013).
924 38. T. Hewezi, T. J. Baum, Manipulation of plant cells by cyst and root-knot nematode
925 effectors. *Mol Plant Microbe Interact* **26**, 9-16 (2013).
926 39. L. Perfus-Barbeoch *et al.*, Elucidating the molecular bases of epigenetic inheritance in
927 non-model invertebrates: the case of the root-knot nematode *Meloidogyne incognita*.
928 *Front Physiol* **5**, 211 (2014).
929 40. R. Hassanaly-Goulamhoussen *et al.*, Chromatin Landscape Dynamics in the Early
930 Development of the Plant Parasitic Nematode *Meloidogyne incognita*. *Front Cell Dev*
931 *Biol* **9**, 765690 (2021).
932 41. M. R. Atighi, B. Verstraeten, T. De Meyer, T. Kyndt, Genome-wide shifts in histone
933 modifications at early stage of rice infection with *Meloidogyne graminicola*. *Molecular*
934 *Plant Pathology* **22**, 440-455 (2021).
935 42. T. Hewezi, Epigenetic Mechanisms in Nematode-Plant Interactions. *Annu Rev*
936 *Phytopathol* **58**, 119-138 (2020).
937 43. L. Pratx *et al.*, Genome-wide expert annotation of the epigenetic machinery of the
938 plant-parasitic nematodes *Meloidogyne* spp., with a focus on the asexually
939 reproducing species. *BMC Genomics* **19**, 321 (2018).
940 44. D. Dai *et al.*, Unzipped chromosome-level genomes reveal allopolyploid nematode
941 origin pattern as unreduced gamete hybridization. *Nature Communications* **14**, 7156
942 (2023).
943 45. C. H. Opperman *et al.*, Sequence and genetic map of *Meloidogyne hapla*: A compact
944 nematode genome for plant parasitism. *Proceedings of the National Academy of*
945 *Sciences* **105**, 14802-14807 (2008).
946 46. P. A. Jones, Functions of DNA methylation: islands, start sites, gene bodies and
947 beyond. *Nature reviews genetics* **13**, 484-492 (2012).
948 47. H. M. Robertson, J. H. Thomas, The putative chemoreceptor families of *C. elegans*.
949 *WormBook* 10.1895/wormbook.1.66.1, 1-12 (2006).
950 48. C. Jiang *et al.*, An expanded subfamily of G-protein-coupled receptor genes in
951 Fusarium graminearum required for wheat infection. *Nat Microbiol* **4**, 1582-1591
952 (2019).
953 49. J. Shang, Y. Shang, G. Tang, C. Wang, Identification of a key G-protein coupled
954 receptor in mediating appressorium formation and fungal virulence against insects. *Sci*
955 *China Life Sci* **64**, 466-477 (2021).
956 50. C. Kumari *et al.*, Molecular characterization of FMRFamide-like peptides in

957 *Meloidogyne graminicola* and analysis of their knockdown effect on nematode
958 infectivity. *Gene* **619**, 50-60 (2017).
959 51. J. Jumper *et al.*, Highly accurate protein structure prediction with AlphaFold. *Nature*
960 **596**, 583-589 (2021).
961 52. N. K. Whiteman, A. D. Gloss, Parasitology: Nematode debt to bacteria. *Nature* **468**,
962 641-642 (2010).
963 53. R. K. Slotkin, R. Martienssen, Transposable elements and the epigenetic regulation of
964 the genome. *Nature reviews genetics* **8**, 272-285 (2007).
965 54. J. D. Hollister, B. S. Gaut, Epigenetic silencing of transposable elements: a trade-off
966 between reduced transposition and deleterious effects on neighboring gene
967 expression. *Genome research* **19**, 1419-1428 (2009).
968 55. S. P. Klein, S. N. Anderson, The evolution and function of transposons in epigenetic
969 regulation in response to the environment. *Curr Opin Plant Biol* **69**, 102277 (2022).
970 56. Y. F. Wei, K. C. Carter, R. P. Wang, B. K. Shell, Molecular cloning and functional
971 analysis of a human cDNA encoding an *Escherichia coli* AlkB homolog, a protein
972 involved in DNA alkylation damage repair. *Nucleic Acids Res* **24**, 931-937 (1996).
973 57. B. I. Fedeles, V. Singh, J. C. Delaney, D. Li, J. M. Essigmann, The AlkB family of Fe
974 (II)/α-ketoglutarate-dependent dioxygenases: repairing nucleic acid alkylation damage
975 and beyond. *Journal of Biological Chemistry* **290**, 20734-20742 (2015).
976 58. T. P. Wu *et al.*, DNA methylation on N(6)-adenine in mammalian embryonic stem cells.
977 *Nature* **532**, 329-333 (2016).
978 59. M. Martin, Cutadapt removes adapter sequences from high-throughput sequencing
979 reads. *EMBnet. journal* **17**, 10-12 (2011).
980 60. B. Langmead, S. L. Salzberg, Fast gapped-read alignment with Bowtie 2. *Nat Methods*
981 **9**, 357-359 (2012).
982 61. H. Li *et al.*, The Sequence Alignment/Map format and SAMtools. *Bioinformatics* **25**,
983 2078-2079 (2009).
984 62. Y. Zhang *et al.*, Model-based analysis of ChIP-Seq (MACS). *Genome Biol* **9**, R137
985 (2008).
986 63. F. Ramirez, F. Dundar, S. Diehl, B. A. Gruning, T. Manke, deepTools: a flexible platform
987 for exploring deep-sequencing data. *Nucleic Acids Res* **42**, W187-191 (2014).
988 64. J. T. Robinson *et al.*, Integrative genomics viewer. *Nature biotechnology* **29**, 24-26
989 (2011).
990 65. P. Machanick, T. L. Bailey, MEME-ChIP: motif analysis of large DNA datasets.
991 *Bioinformatics* **27**, 1696-1697 (2011).
992 66. S. Koren *et al.*, Canu: scalable and accurate long-read assembly via adaptive k-mer
993 weighting and repeat separation. *Genome Res* **27**, 722-736 (2017).
994 67. H. Li, R. Durbin, Fast and accurate short read alignment with Burrows-Wheeler
995 transform. *Bioinformatics* **25**, 1754-1760 (2009).
996 68. A. Tarasov, A. J. Vilella, E. Cuppen, I. J. Nijman, P. Prins, Sambamba: fast processing
997 of NGS alignment formats. *Bioinformatics* **31**, 2032-2034 (2015).
998 69. B. J. Walker *et al.*, Pilon: an integrated tool for comprehensive microbial variant
999 detection and genome assembly improvement. *PLoS One* **9**, e112963 (2014).
1000 70. N. C. Durand *et al.*, Juicer Provides a One-Click System for Analyzing

1001 Loop-Resolution Hi-C Experiments. *Cell Syst* **3**, 95-98 (2016).
1002 71. O. Dudchenko *et al.*, De novo assembly of the *Aedes aegypti* genome using Hi-C
1003 yields chromosome-length scaffolds. *Science* **356**, 92-95 (2017).
1004 72. J. M. Flynn *et al.*, RepeatModeler2 for automated genomic discovery of transposable
1005 element families. *Proc Natl Acad Sci U S A* **117**, 9451-9457 (2020).
1006 73. N. Chen, Using Repeat Masker to identify repetitive elements in genomic sequences.
1007 *Current protocols in bioinformatics* **5**, 4.10. 11-14.10. 14 (2004).
1008 74. D. Kim, J. M. Paggi, C. Park, C. Bennett, S. L. Salzberg, Graph-based genome
1009 alignment and genotyping with HISAT2 and HISAT-genotype. *Nat Biotechnol* **37**,
1010 907-915 (2019).
1011 75. M. Stanke *et al.*, AUGUSTUS: ab initio prediction of alternative transcripts. *Nucleic*
1012 *acids research* **34**, W435-W439 (2006).
1013 76. A. Lomsadze, V. Ter-Hovhannisyan, Y. O. Chernoff, M. Borodovsky, Gene
1014 identification in novel eukaryotic genomes by self-training algorithm. *Nucleic acids*
1015 *research* **33**, 6494-6506 (2005).
1016 77. T. Bruna, K. J. Hoff, A. Lomsadze, M. Stanke, M. Borodovsky, BRAKER2: automatic
1017 eukaryotic genome annotation with GeneMark-EP+ and AUGUSTUS supported by a
1018 protein database. *NAR Genom Bioinform* **3**, lqaa108 (2021).
1019 78. B. J. Haas *et al.*, De novo transcript sequence reconstruction from RNA-seq using the
1020 Trinity platform for reference generation and analysis. *Nature protocols* **8**, 1494-1512
1021 (2013).
1022 79. B. J. Haas *et al.*, Automated eukaryotic gene structure annotation using
1023 EVidenceModeler and the Program to Assemble Spliced Alignments. *Genome biology*
1024 **9**, 1-22 (2008).
1025 80. R. D. Finn, J. Clements, S. R. Eddy, HMMER web server: interactive sequence
1026 similarity searching. *Nucleic acids research* **39**, W29-W37 (2011).
1027 81. J. Huerta-Cepas *et al.*, Fast genome-wide functional annotation through orthology
1028 assignment by eggNOG-mapper. *Molecular biology and evolution* **34**, 2115-2122
1029 (2017).
1030 82. J. J. Almagro Armenteros *et al.*, SignalP 5.0 improves signal peptide predictions using
1031 deep neural networks. *Nature biotechnology* **37**, 420-423 (2019).
1032 83. S. Möller, M. D. Croning, R. Apweiler, Evaluation of methods for the prediction of
1033 membrane spanning regions. *Bioinformatics* **17**, 646-653 (2001).
1034 84. S. Ou *et al.*, Benchmarking transposable element annotation methods for creation of a
1035 streamlined, comprehensive pipeline. *Genome biology* **20**, 1-18 (2019).
1036 85. A. R. Quinlan, I. M. Hall, BEDTools: a flexible suite of utilities for comparing genomic
1037 features. *Bioinformatics* **26**, 841-842 (2010).
1038 86. G. Yu, L.-G. Wang, Q.-Y. He, ChIPseeker: an R/Bioconductor package for ChIP peak
1039 annotation, comparison and visualization. *Bioinformatics* **31**, 2382-2383 (2015).
1040 87. M. Krzywinski *et al.*, Circos: an information aesthetic for comparative genomics.
1041 *Genome Res* **19**, 1639-1645 (2009).
1042 88. B. Li, C. N. Dewey, RSEM: accurate transcript quantification from RNA-Seq data with
1043 or without a reference genome. *BMC bioinformatics* **12**, 1-16 (2011).
1044 89. S. Anders, P. T. Pyl, W. Huber, HTSeq—a Python framework to work with

1045 high-throughput sequencing data. *bioinformatics* **31**, 166-169 (2015).
1046 90. M. I. Love, W. Huber, S. Anders, Moderated estimation of fold change and dispersion
1047 for RNA-seq data with DESeq2. *Genome biology* **15**, 1-21 (2014).
1048 91. L. Kumar, M. E. Futschik, Mfuzz: a software package for soft clustering of microarray
1049 data. *Bioinformation* **2**, 5 (2007).
1050 92. S. F. Altschul *et al.*, Gapped BLAST and PSI-BLAST: a new generation of protein
1051 database search programs. *Nucleic acids research* **25**, 3389-3402 (1997).
1052 93. R. Horsch *et al.*, A simple and general method for transferring genes into plants.
1053 *science* **227**, 1229-1231 (1985).
1054

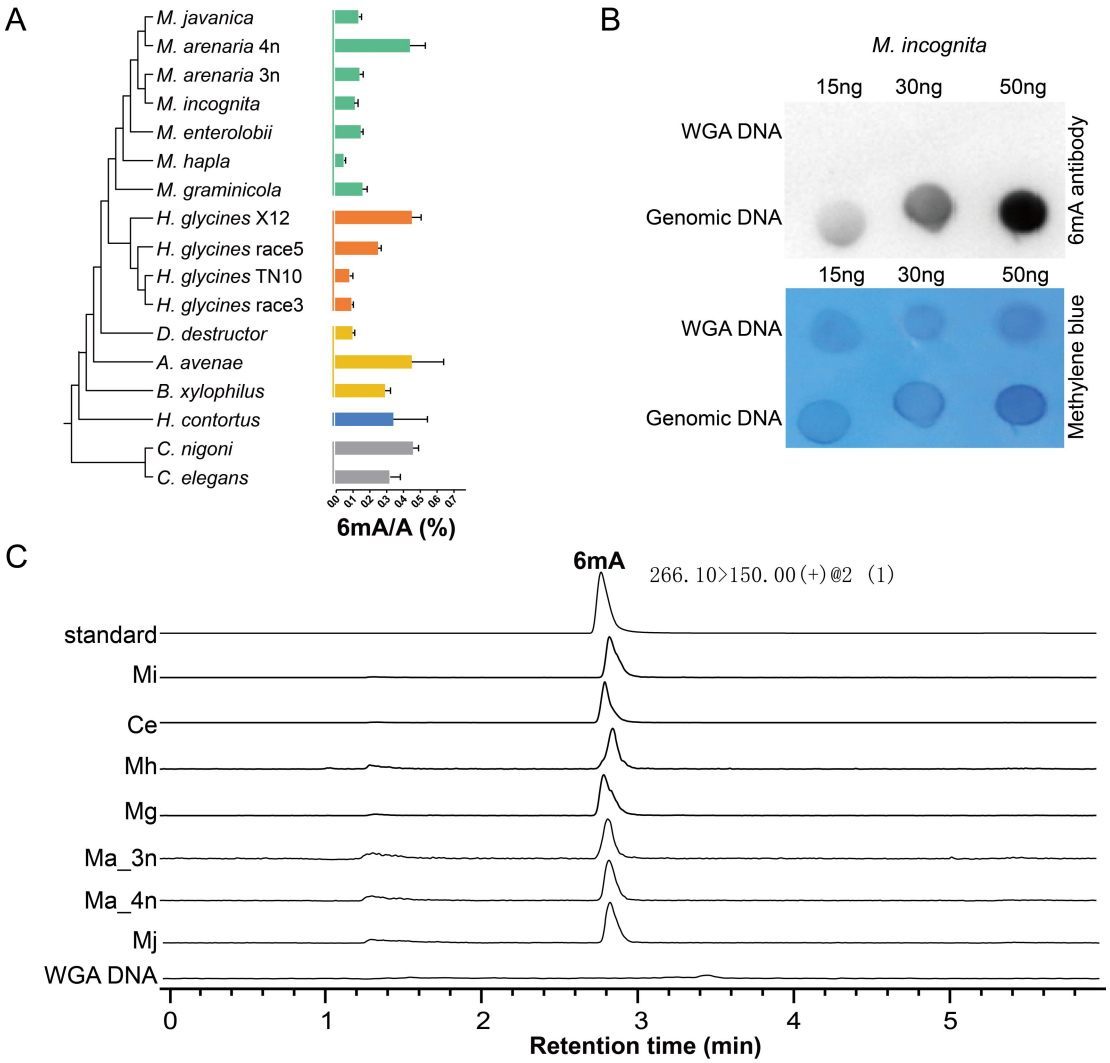

Figure 1. 6mA DNA methylation is widespread in nematode. (*A*), 6mA levels identified by LC-MS/MS in different nematodes. The green bar plot means 7 species of RKNs, the orange bar plot means 4 isolates of cyst nematodes, the yellow bar plot means migratory nematodes, the blue bar plot means animal-parasitic nematode, and the gray bar plot means free-living nematode. Three biological replicates per species. (*B*), The DNA 6mA Dot blot of *M. incognita,* the figure below shows the membrane after antibody hybridization and chemiluminescence, and then methylene blue staining. Whole genome amplified (WGA) DNA of the *M. incognita* genome, generated using Phi29 polymerase, was used as a negative control. (*C*), LC-MS/MS for 6mA standard and 6mA levels in genomic DNA purified from *M. incognita*, *C. elegans*, *M. hapla* (Mh), *M. graminicola* (Mg), *M. arenaria* 3n (Ma 3n), *M. arenaria* 4n (Ma 4n), and *M. javanica* (Mj), respectively. The WGA DNA was used as a negative control. All DNAs were extracted from nematode eggs.

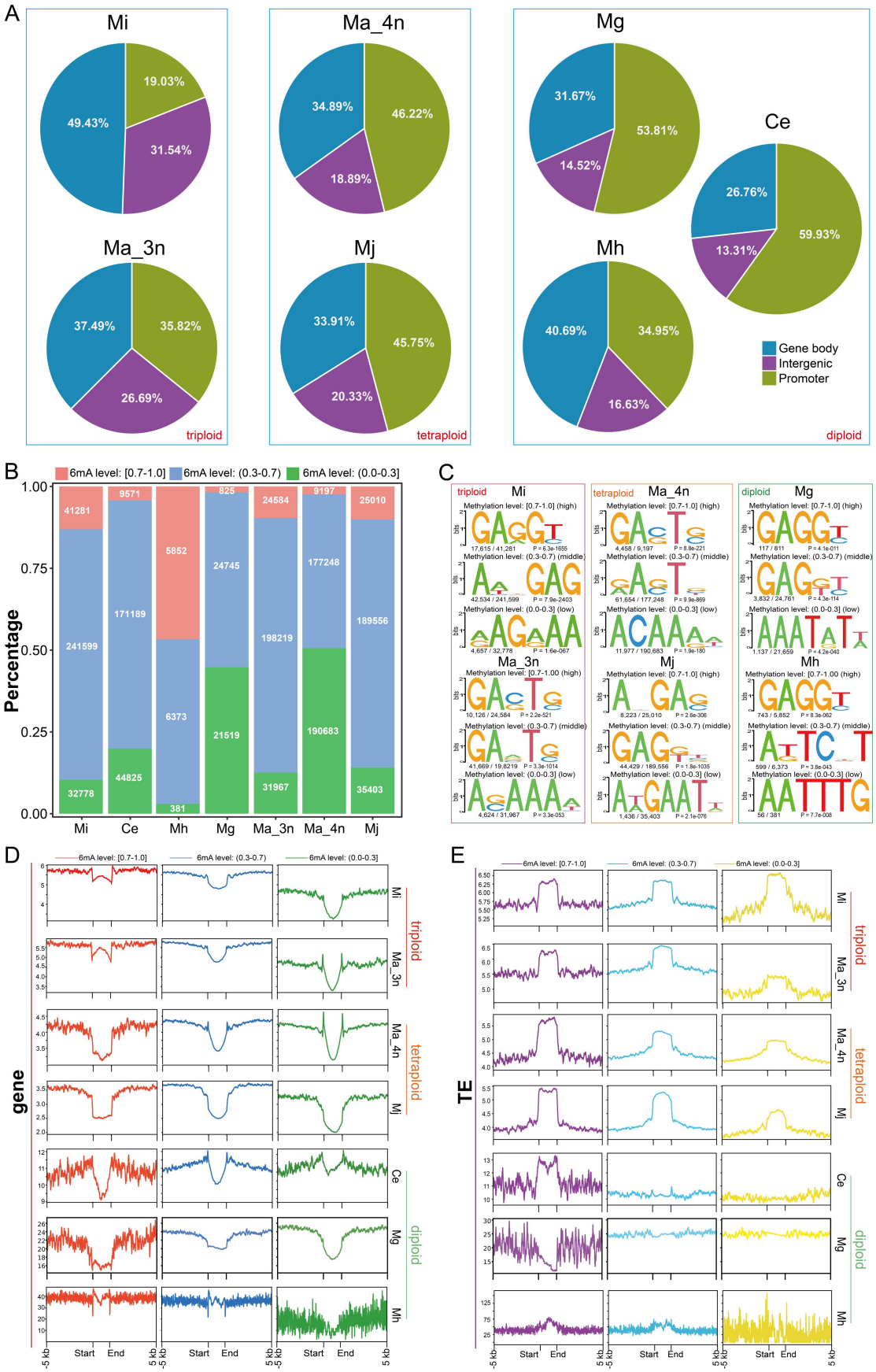

Figure 2. The distribution landscape of 6mA in RKNs genome. (*A*), The distribution ratio of 6mA in three nematodes promoter, gene body, and intergenic. *M. incognita* (Mi), *M. arenaria*

1071 3n (Ma 3n), *M. arenaria* 4n (Ma 4n), *M. javanica* (Mj), *M. graminicola* (Mg), *M. hapla* (Mh), and
1072 *C. elegans*. The 1 kb region before the start codon is defined as the promoter. (*B*), Percentage
1073 of the different modification level categories of 6mA in Mi, Ma 3n, Ma 4n, Mj, Mg, and Mh,
1074 respectively. (*C*), The motif of different methylation categories of Mi, Ma 3n, Ma 4n, Mj, Mg,
1075 and Mh. (*D*) The distribution density of 6mA on gene regions within 100bp genome window (Mi,
1076 Ma 3n, Ma 4n, Mj, Ce, Mg, and Mh). (*E*) The distribution density of 6mA on transposable
1077 element (TE) region within 100bp genome window. *p* values were calculated by two-sided
1078 Wilcoxon rank sum tests. The y-axis represents the average number of 6mA per 100 bp
1079 genome window.
1080
1081

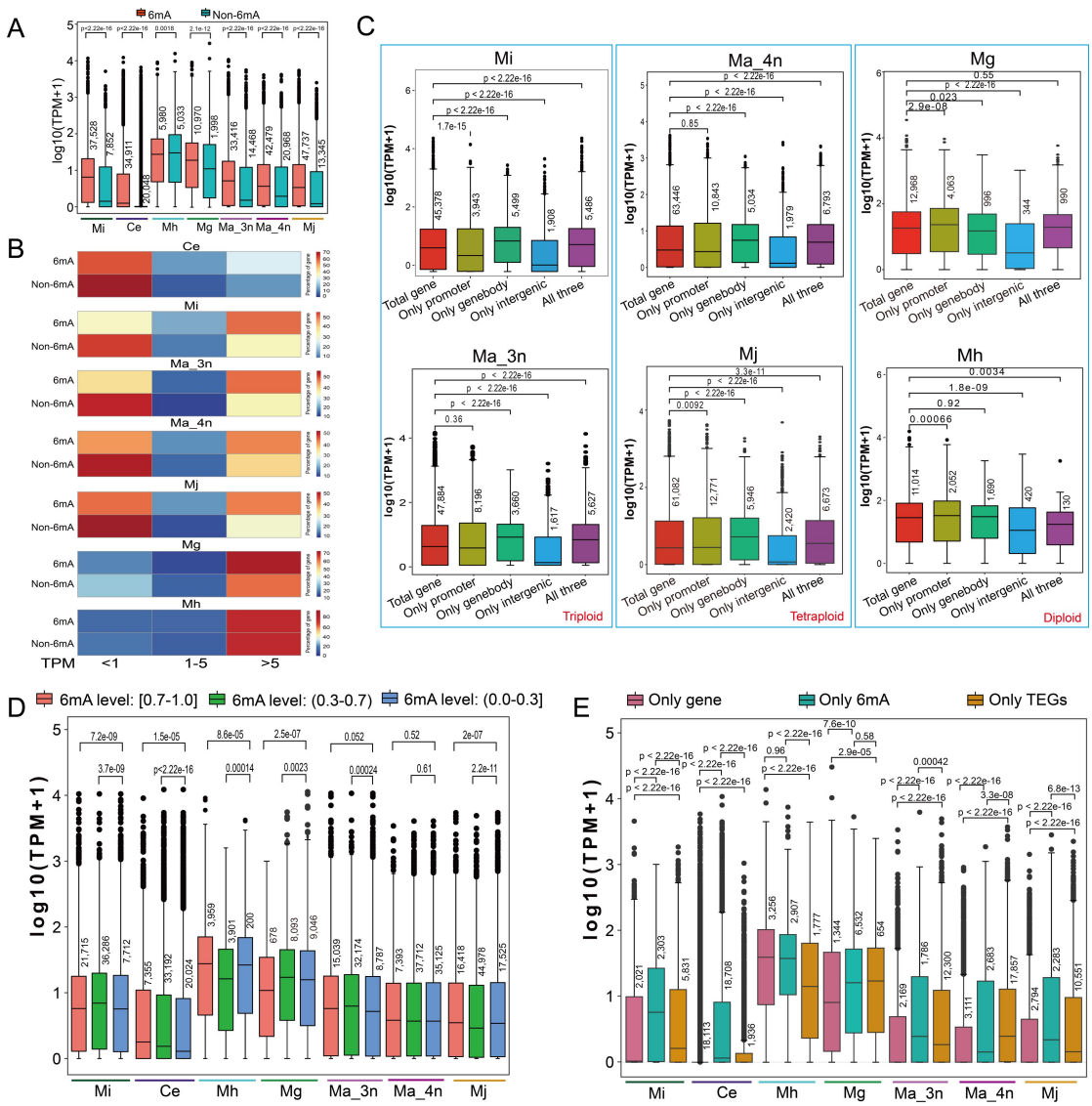

Figure 3. 6mA influences the genes expression level of nematodes. (*A*) The comparison of TPM value between 6mA-methylated (6mA) and unmethylated (Non-6mA) in Ce, Mi, Ma, Mj, Mg, and Mh. The gene with 6mA modification in the promoter, gene body, or intergenic region was defined as a 6mA-modified gene; otherwise, it was classified as an unmethylated gene. (*B*) The percentage of 6mA-methylated (6mA) and unmethylated (Non-6mA) genes at a given TPM level (<1, 1–5, and >5). (*C*) The comparison of expression levels between the genes modified by 6mA at different positions and total genes. (*D*) The comparison of genes expression level of different 6mA modification level categories in Mi, Ma 3n, Ma 4n, Mj, Ce, Mg, and Mh. (*E*) Gene expression in Mi, Mh, Mg, Ma 3n, Ma 4n, and Mj categorized into three groups: genes modified only by 6mA without nearby TE ("only 6mA"), genes associated only with nearby TE but lacking 6mA ("only TE"), and genes with neither 6mA modification nor nearby TE ("only gene"). In box plots, the central line represents the median, the box represents the 25% and 75% percentiles, and the whiskers represent 1.5 times the interquartile range beyond the box. N numbers were shown upon the box. *p* values were calculated by two-sided Wilcoxon rank sum tests.

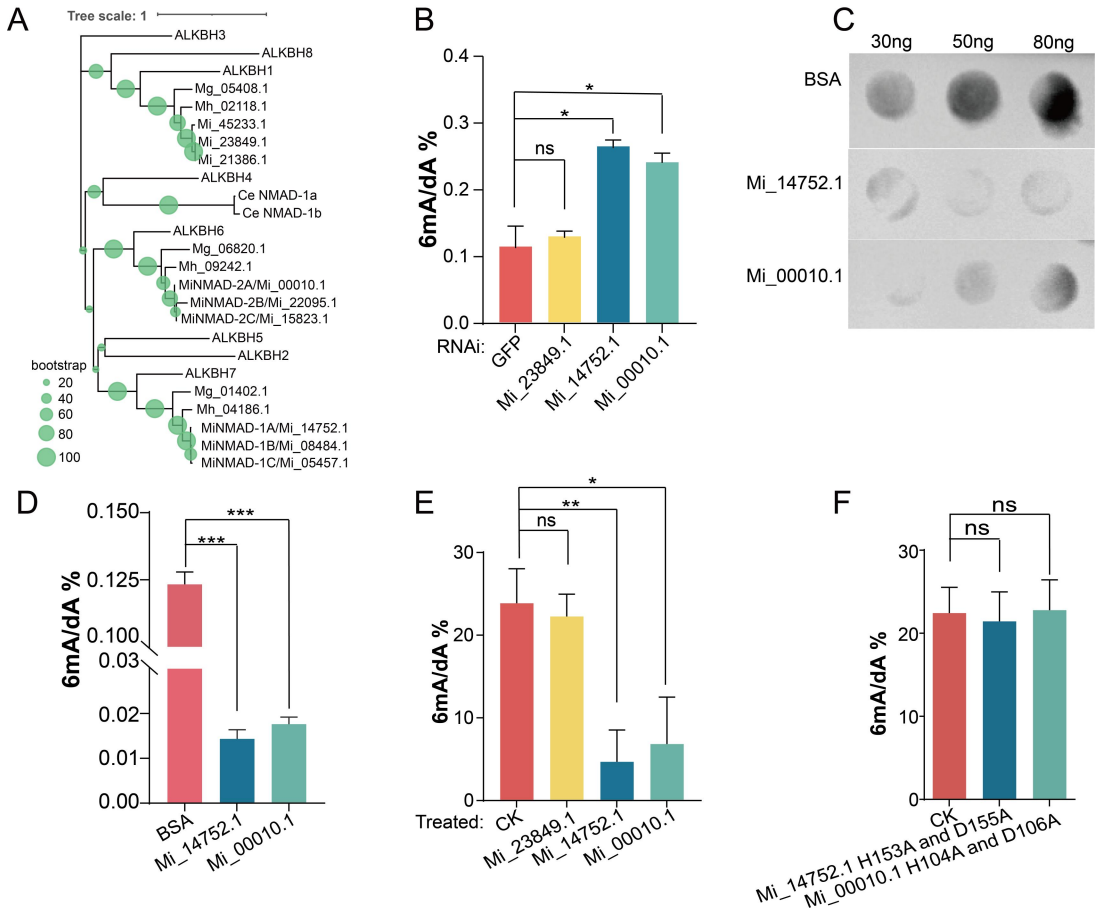

Figure 4. MiNMAD-1/2 are involved in 6mA demethylation in *M. incognita*. (*A*), The maximum-likelihood tree is constructed from the protein sequence of RKNs, *C. elegans* demethylase, and human ALKBH family members, bootstraps are shown in green dot. (*B*), Knockdown of 3 ALKBH family members present a significant increase of 6mA level in two of them (Mi_14752.1, Mi_00010.1). (*C*), In vitro demethylation assay showing that purified Mi_14752.1 and Mi_00010.1 proteins catalyze the removal of DNA methylation from Mi WHF4-1 egg genomic DNA, with BSA included as a negative control. (*D*), The 6mA contents of (*C*) were determined by LC-MS/MS. (*E*), LC-MSMS detected the oligo DNA with 6mA modified (G**A**G) was demethylated by purified MiNMAD-1/2 proteins *in vitro*. (*F*), Mutation of the catalytic domain of Mi_14752.1 and Mi_00010.1 abrogates the ability of them to demethylate 6mA premethylated oligos. *p* values were calculated by two-tailed unpaired Student's *t*-test. One star * means $p < 0.05$, two means $p < 0.01$, three means $p < 0.001$.

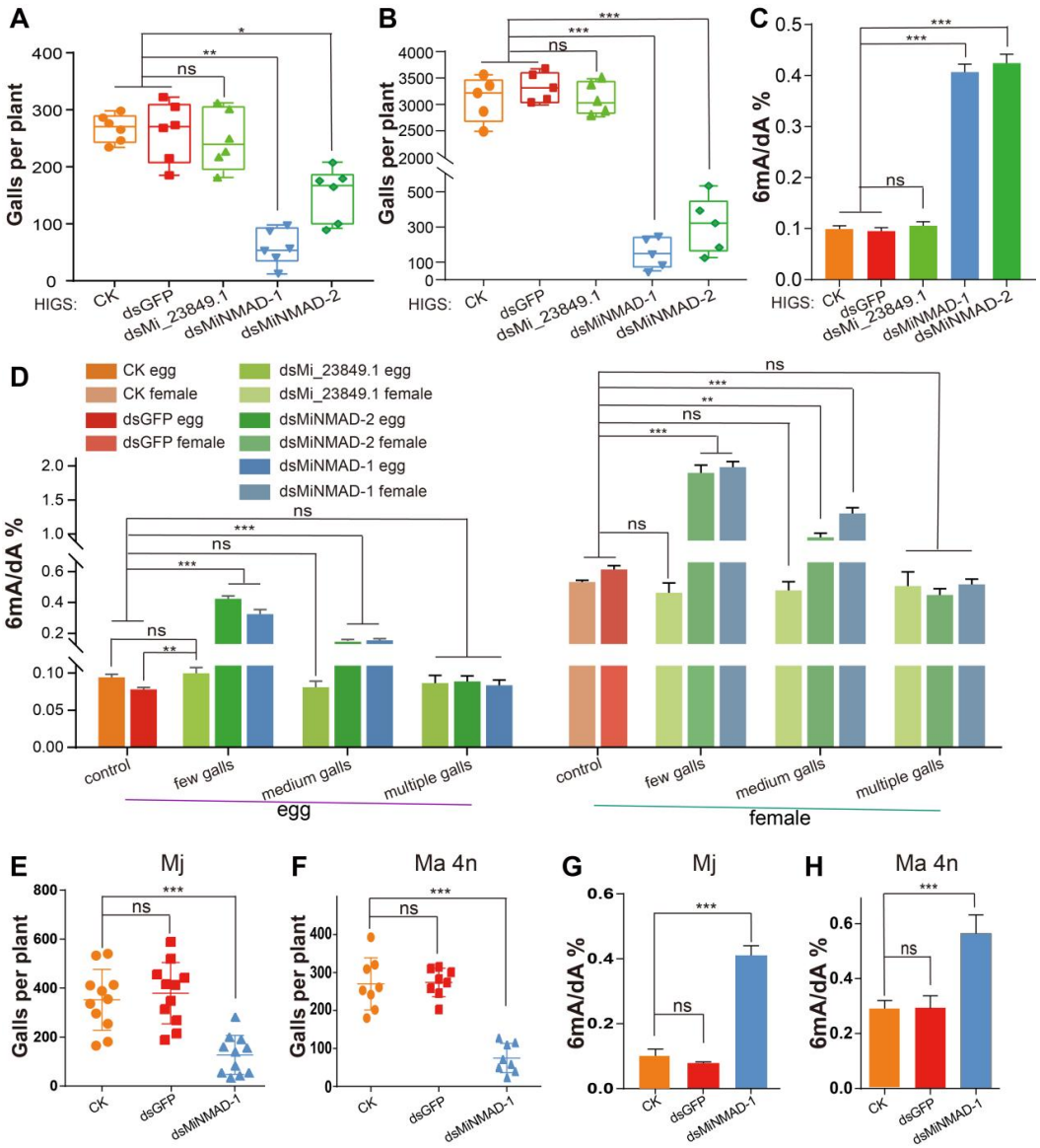

Figure 5. Host-induced gene silencing of *minmad-1* reduces the infectivity of polyploid RKNs. (*A*) Three weeks pot experiment of transgenic plants show a resistance of Mi for *minmad-1/2* RNAi, but no difference for *Mi_23849.1* RNAi. (*B*) Eight weeks pot experiment show an extremely significant resistance of expression *MiNMAD-1/2* dsRNA transgenic tobacco to Mi. (*C*) The 6mA level of Mi is significantly increased after infection of transgenic tobacco expression *minmad-1/2* dsRNA. (*D*) The number of galls was proportional to the methylation content in the corresponding Mi, and the level of 6mA in females was much higher than in eggs. (*E*) The number of galls after 1000 *M. javanica* (Mj) J2 infection two months of transgenic tobacco expressing *minmad-1* dsRNA. (*F*) The number of root-knots after 1000 M. arenaria 4n (Ma 4n) J2 infection of two months of transgenic tobacco expressing minmad-1 dsRNA. (*G*) The genomic DNA 6mA content of the Mj after infecting the *minmad-1* transgenic tobaccos was significantly higher than that of the control. (*H*) The genomic DNA 6mA content of the Ma 4n after infecting the *minmad-1* transgenic tobaccos was significantly higher than that of the control. *p* values were calculated by two-tailed unpaired Student's *t*-test. One star * means $p < 0.05$, two means $p < 0.01$, three means $p < 0.001$.

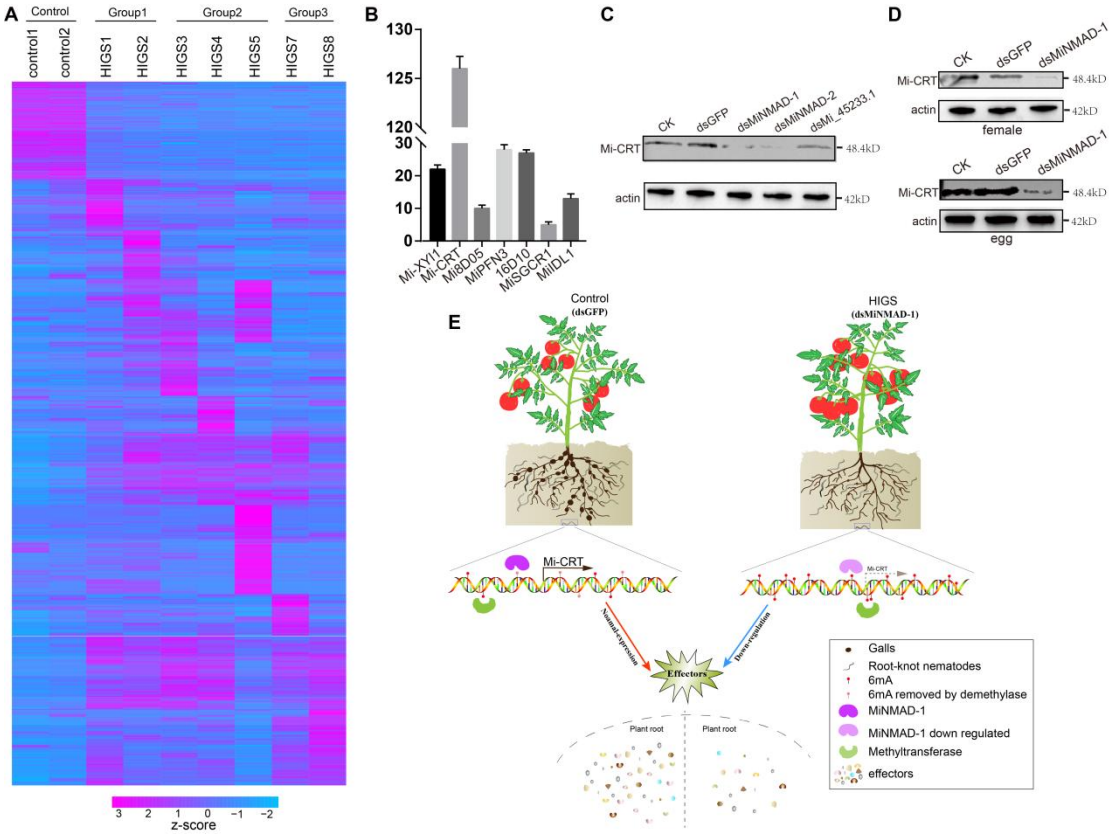

Figure 6. 6mA regulation of the expression module of *M. incognita* effector. (*A*) The Expression patterns of all secreted proteins at Mi J3J4 stage in dsGFP control group and *minmad-1/2* RNAi group. Group1: multiple-galls. Group2: medium-galls. Group3: low-galls. (*B*) Relative fold down-regulation of some validated effectors after HIGS of *minmad-1*, assay was performed by qRT-PCR in Mi female. (*C*) Western blot of the highest down-regulate effector show that Mi-CRT was also significantly down-regulated at the protein level after *minmad-1/2* RNAi. (*D*) Mi-CRT protein level down-regulate both at egg and female stage. (*E*) Schematic illustration of the regulation of Mi virulence factor expression patterns by 6mA to affect the ability of nematode infectivity.